Office of Naval Research

Contract Nonr-1866(16) NR-372-012

INTERACTION OF SIGNAL AND NOISE IN A NONLINEAR SYSTEM

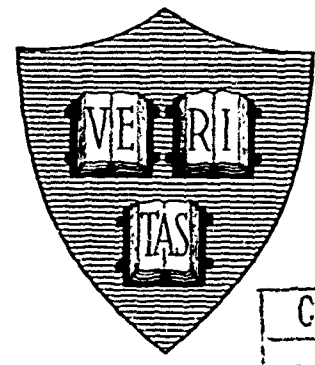

By

P. Trafton and D. W. Tufts

July 27, 1964

Technical Report No. 450

Cruft Laboratory

Division of Engineering and Applied Physics

Harvard University • Cambridge, Massachusetts

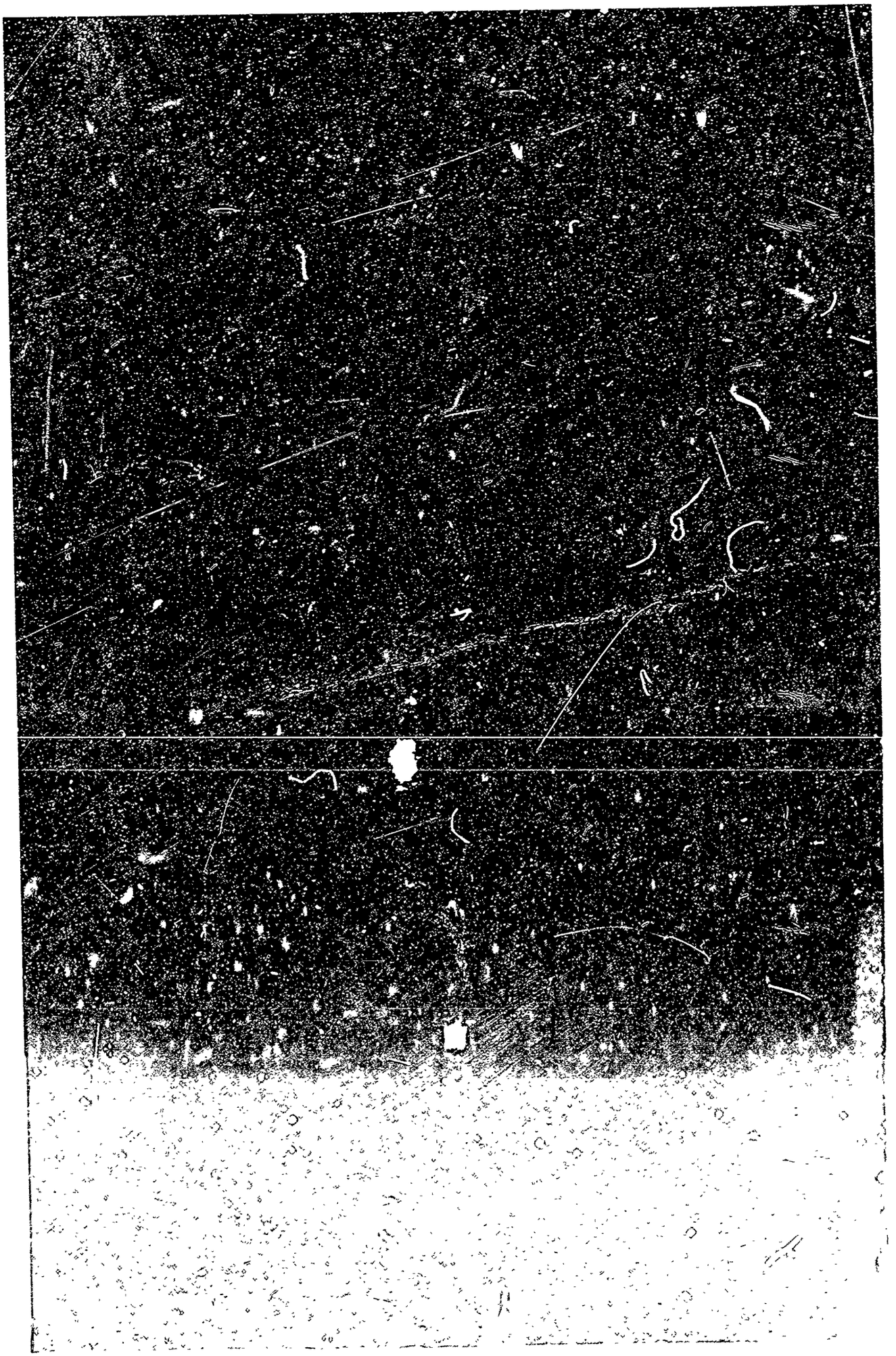

Office of Naval Research

Contract Nonr-1866(16)

NR - 372 - 012

INTERACTION OF SIGNAL AND NOISE IN A NONLINEAR SYSTEM

by

P. Trafton and D. W. Tufts

July 27, 1964

The research reported in this document was made possible through support extended to Cruft Laboratory, Harvard University, by the U. S. Army Research Office, the U. S. Air Force Office of Scientific Research, and the U. S. Office of Naval Research under the Joint Services Electronics Program by Contract Nonr-1866(16). Reproduction in whole or in part is permitted for any purpose of the United States Government.

Technical Report No. 450

Cruft Laboratory

Division of Engineering and Applied Physics

Harvard University

Cambridge, Massachusetts

ABSTRACT

An experimental system has been constructed which simulates the detection stage of a receiver. With the application of periodic bursts of sine-wave plus Gaussian noise at the input, the output of this system is a non-stationary random process. The addition of noise to the signal suppresses the mean at the output for the half-wave linear detector. However, the mean is unchanged for the half-wave square-law detector. The non-stationary variance is seen to vary between two values which can be easily measured. Output signal-to-noise ratio is greater for the half-wave square-law device than for the half-wave linear device. Addition of a clipper to the half-wave linear device decreases the signal-to-noise ratio. Detection characteristics of the half-wave linear and half-wave square-law devices are found to be equivalent and the clipper degrades the detection characteristic.

INTERACTION OF SIGNAL AND NOISE IN A NONLINEAR SYSTEM

by

P. Trafton and D. W. Tufts

Division of Engineering and Applied Physics

Harvard University, Cambridge, Massachusetts

I. INTRODUCTION

A classical problem in communication theory is the specification of the random output of two linear filters separated by a zero-memory, nonlinear element when excited by noise and signal plus noise, as shown in Fig. 1 below.

FIG. 1. Model of a Nonlinear Filter

In most problems of interest, the first filter is a narrow-band filter which is centered at a high frequency, and the second is a low-pass filter. The noise, $n(t)$, is assumed to have Gaussian statistics, and the signal, $s(t)$, is often a burst of sine-wave.

The analytical problems encountered in this type of problem are very formidable and only limited theoretical results are available. For example, the problem of finding the output amplitude distribution function is, in general, unsolved. In most cases, the first two moments of the output can be found only approximately, and then only with difficulty.

Considerable theory exists for so-called envelope detectors with Gaussian inputs. In this situation, the output of the narrow-band filter is represented in the form $E(t)\cos[\omega_o t + a(t)]$, where ω_o is the center frequency of the filter. The random envelope and random phase of the process are $E(t)$ and $a(t)$, respectively. The distribution function of $E(t)$ is known when the input consists of Gaussian noise or sine-wave plus Gaussian noise. With noise alone, $E(t)$ has a Rayleigh distribution; and for sine-wave plus noise, $E(t)$ has a modified Rayleigh distribution. An "envelope detector" is assumed to recover $E(t)$ or some power of $E(t)$ at its output. Thus, the output statistics are known. A half-wave linear element followed by an ideal low-pass filter can function as an envelope detector, if the low-pass filter passes $E(t)$ exactly and rejects all harmonics of the input. This theory, however, is not applicable if, for example, the low-pass filter does some filtering of $E(t)$. Also, this theory is not applicable if the nonlinear element is other than linear or square-law. Both these situations are explored in this report.

Power spectrum analyses of this system have been made by Rice [1] and Middleton [8], among others, and the essential results are given by Davenport and Root [2]. These analyses lead to series approximations, in most cases, for the auto-correlation functions and low-frequency power spectra. From this, the first two moments may be obtained. Experimental measurements of the low-frequency auto-correlation function and power spectrum for a variety of non-linearities have been performed by Johnson and Fellows under the direction of Middleton [8]. In all the above investigations, the input is often Gaussian noise or sine-wave plus Gaussian noise.

Attempts to find the output density functions have been made in a series of papers by Kac, Siegert, and Emerson [3, 4, 5] . For a square-law nonlinearity, Kac and Siegert obtain the output characteristic function but inversion of it is extremely difficult. Emerson obtains the output cumulants and uses these to approximate the density function by a series with Gaussian noise and sine-wave plus Gaussian noise as inputs. The filters are assumed t have Gaussian-shaped amplitude responses.

In view of the analytical difficulties in this area, an experimental apparatus has been constructed. This apparatus permits us to study various attributes of the random output of Fig. 1 and, in particular, the first two moments and the amplitude distribution function. A wide range of nonlinearities are being considered.

II. SYSTEM DESCRIPTION

The diagram in Fig. 2 illustrates the experimental system that is being studied. The time base for the system is a 1 Kc pulse train produced by the counter. This pulse train acts as an external trigger for the pulse generator which then produces two pulse trains. One of these is a periodic 1 Kc sequence of rectangular pulses of controllable width which triggers a gate circuit. Since the input to the gate is a continuous 130 Kc sine-wave, the output, $s(t)$, of the gate is a periodic burst of sine-wave. This is the signal. The second pulse train produced by the pulse generator is delayed with respect to the first. This delayed pulse train triggers the sampler at

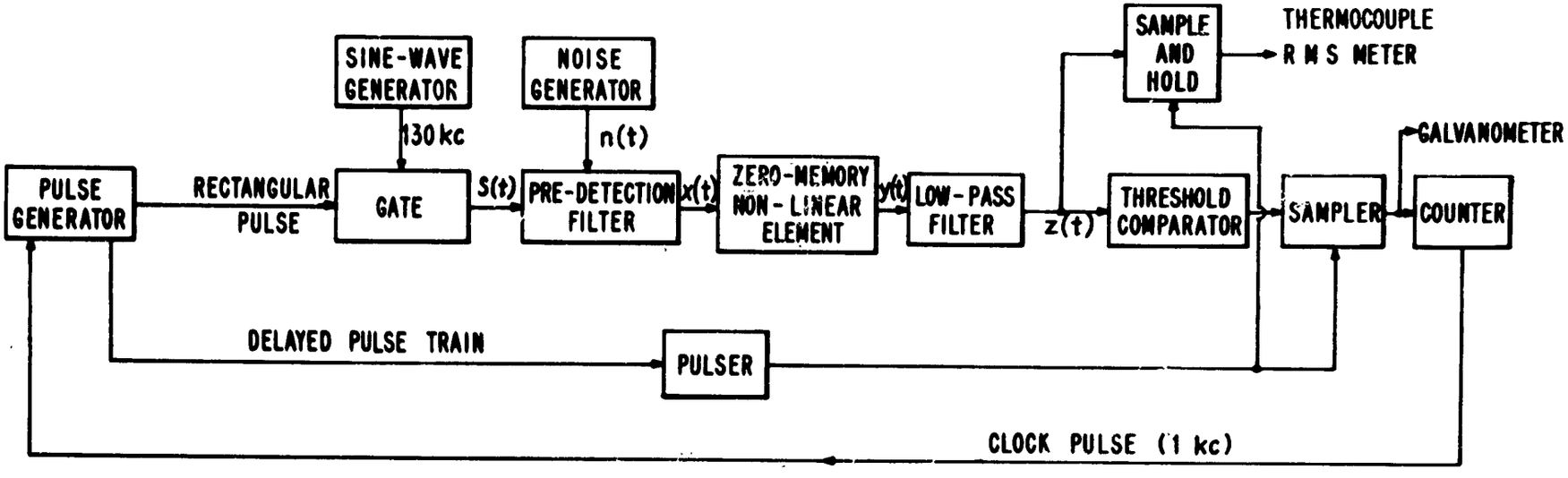

FIG. 2 SYSTEM DIAGRAM

the output of the system. Thus, the output may be sampled at any point in time with respect to the time of occurrence of the leading edge of a signal pulse.

The pre-detection filter and low-pass filter are characterized by their amplitude frequency response curves and examples of these are shown in Figs. 3 and 4. The pre-detection filter consists of two second-order tuned circuits in series and the low-pass filter is fourth-order (SKL Model 302). Both filters have adjustable bandwidths. The pre-detection filter performs an adding operation so that its output, $x(t)$, is a sum of filtered signal plus noise. Also, for the low-pass filter, $|H(0)| = 0$; i.e., there is no transmission at zero frequency.

The stationary noise voltage, $n(t)$, is generated by a gas tube and is very nearly Gaussian. It is not exactly Gaussian because extremely large voltage excursions are clipped, an unavoidable effect in an actual physical system. Its power spectrum is flat across the frequency range of the pre-detection filter.

The nonlinear element is realized by a so-called photo-former. This is a unit in which a cathode-ray oscilloscope tube (CRT) is the main component. The following diagram illustrates its operation.

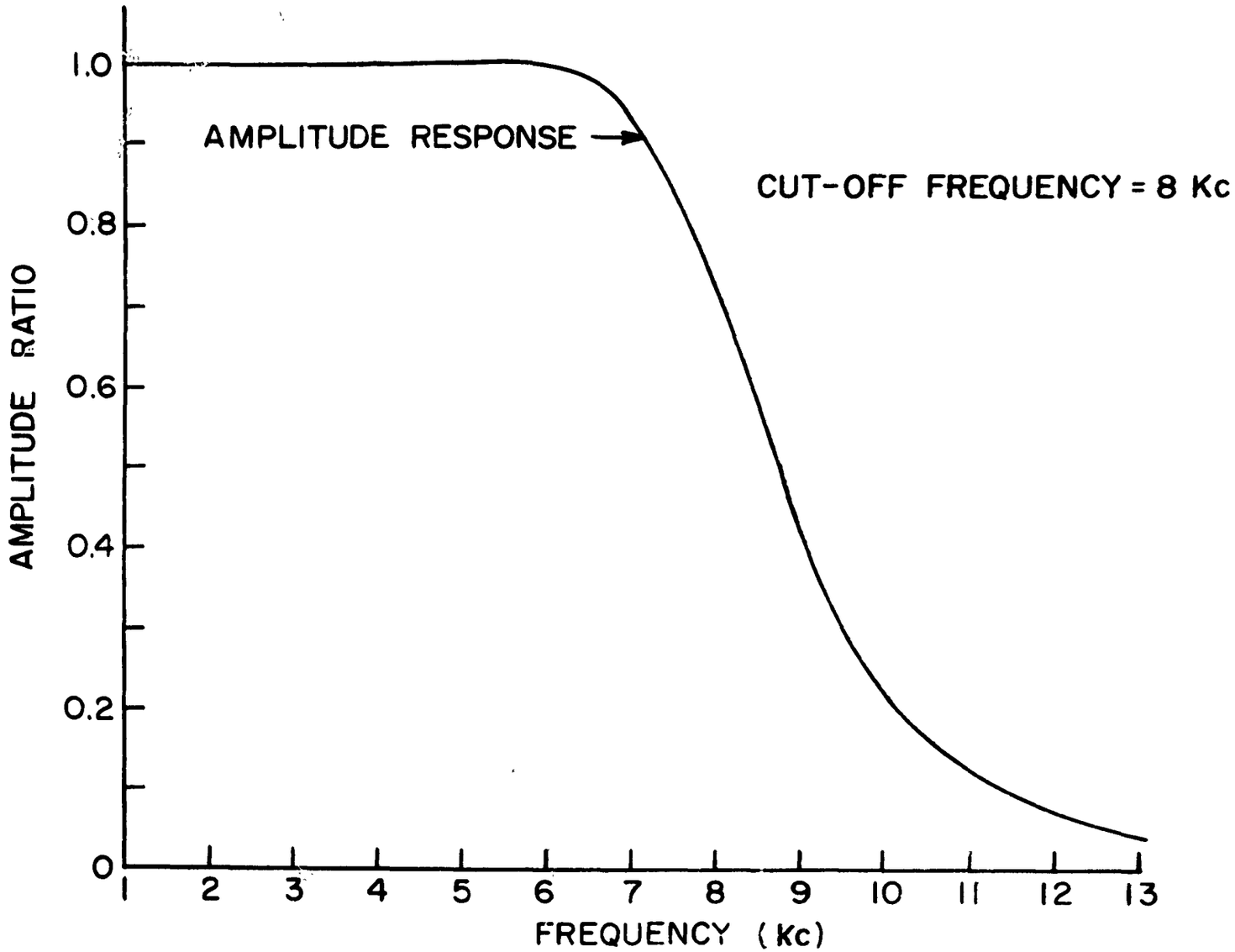

FIG. 3 FREQUENCY RESPONSE OF LOW-PASS FILTER.

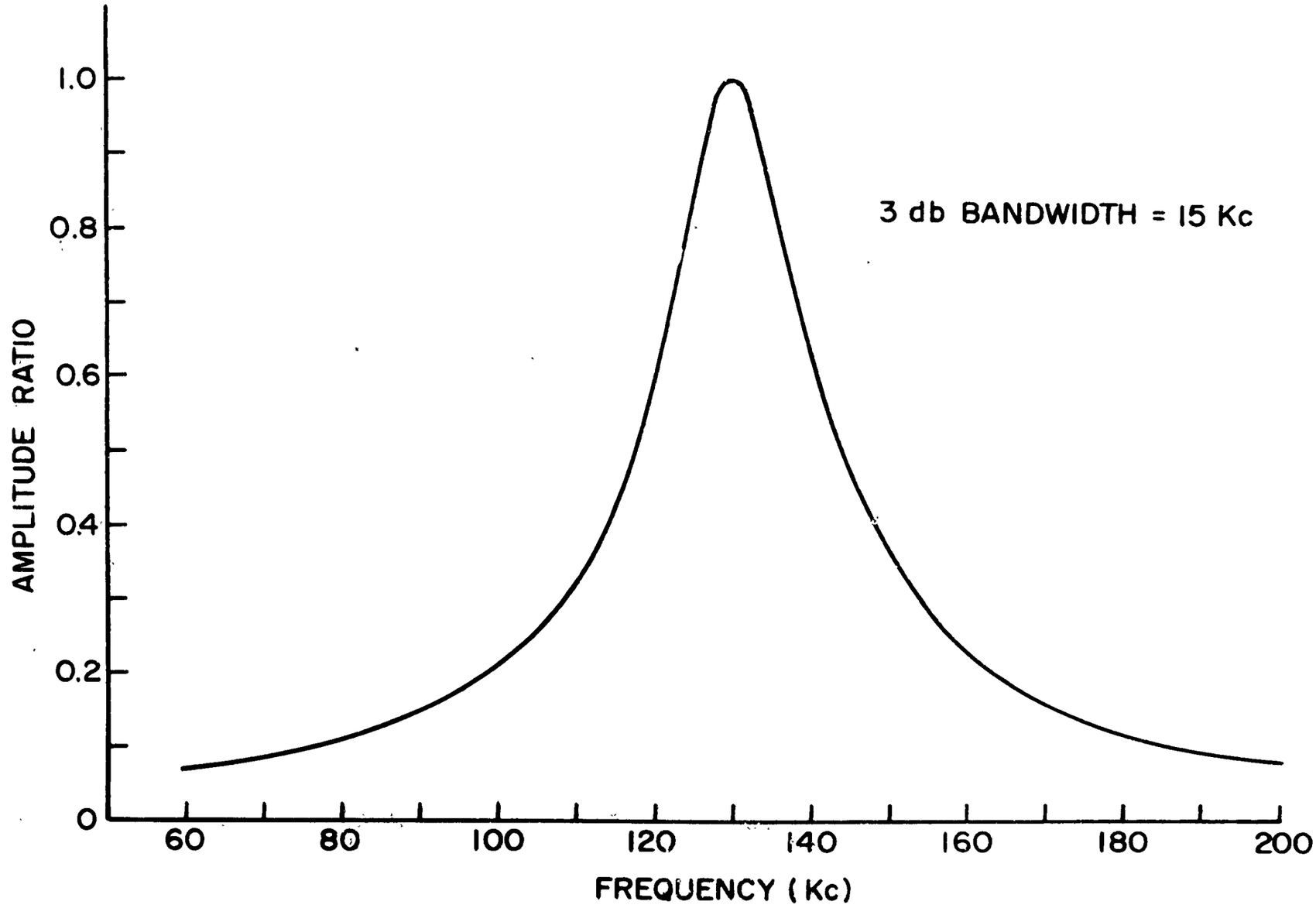

FIG. 4 AMPLITUDE RESPONSE OF PRE-DETECTION FILTER.

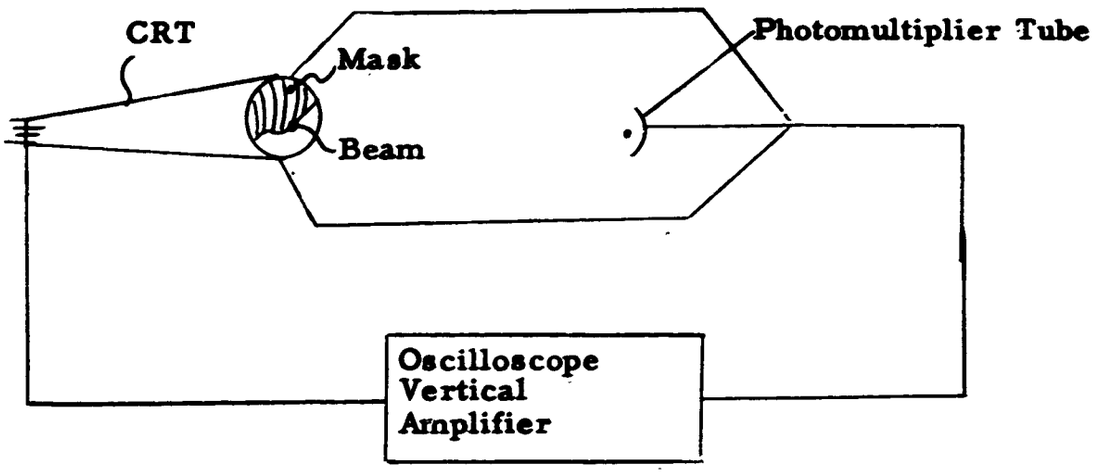

FIG. 5 Photo-former Circuit

The CRT spot is positioned to be just below the edge of the mask. If the spot moves lower, the increased light reaching the photo-tube moves the spot up. If the spot moves up behind the mask, the reduced light moves the spot down. The spot, therefore, stays at the edge of the mask. As the spot is swept horizontally by the oscilloscope sweep circuit, it follows the edge of the mask, tracing out the pattern. Any arbitrary function can be generated by cutting out the proper mask and placing it over the CRT face. The input signal plus noise is then applied to the horizontal input and the output waveform is then obtained from the vertical output. This unit has been found to work satisfactorily if the input frequency is moderate (less than 200 Kc).

The elements following the low-pass filter are used in performing measurements and will be discussed in the next section.

III. MEASUREMENT TECHNIQUES

1. Measurement of the Amplitude Distribution Function

If a fixed periodic signal plus stationary noise is applied to the input of the system of Fig. 1, then the output is a non-stationary random process. Thus, the amplitude distribution function varies as the sampling instant is varied, and in our case (cf. Fig. 2) this variation is periodic. The measurement is performed by using a threshold comparator, sampler, and counter as shown in Fig. 2. The threshold comparator can be set either to pass the output waveform unchanged except for an arbitrary dc voltage added or it supplies a controllable dc voltage to the sampler. In this latter case, the sampler (a high-speed transistor gate of 2μ sec duration) samples a dc voltage at a 1 Kc rate. The threshold on the counter is then adjusted to count at this level. Then the random waveform is applied to the sampler and the counter indicates the number of samples out of 10,000 that exceed the threshold (there is a 10 sec counting interval). Thus, we have an experimental measurement of $1-F(z)$ at some time t from which $F(z)$ is obtained where $F(z)$ is the amplitude distribution function. By varying the threshold settings, we obtain $F(z)$ over the range of interest. Then the sampling time is changed and the measurement is repeated. Thus we measure the evolution in time of the amplitude distribution function.

2. Measurement of the Mean

In the presence of periodic signal plus stationary noise at the input, the mean value of the output of Fig. 1 also varies periodically in time. The

measurement of the mean can be done very simply by passing the samples of Fig. 2 directly into a sensitive galvanometer. A simple calibration is performed by passing samples of fixed and known amplitudes into the galvanometer.

3. Measurement of the Variance

The variance of the output of Fig. 1 is also a periodic non-stationary function. The measurement of the non-stationary variance of the samples is somewhat more difficult than measurement of the mean or amplitude distribution function and requires special instrumentation. This is because it is very difficult to find an instrument that can perform accurate power measurements on pulses that are very narrow compared with their amplitudes. Measurement of the variance is, of course, a power measurement. To circumvent this problem, a sample and hold circuit (cf. Fig. 2) is employed. This preserves the amplitude but extends the duration of the samples and it is relatively easy to find an RMS meter that can perform accurate measurements on this new waveform. The following diagram illustrates the operation of the sample and hold circuit.

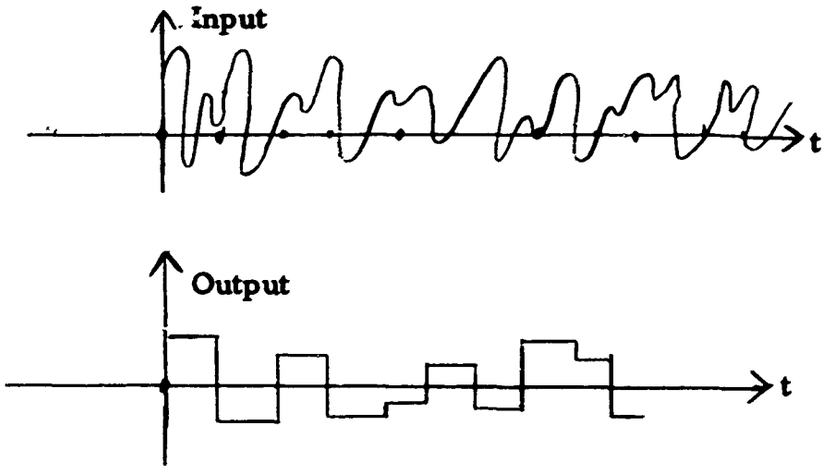

FIG. 6 Input and Output Waveforms of Sample and Hold Circuit

Sampling is performed once every 1 m sec. The sampling duration is 2 μ sec and the hold duration is 998 μ sec. Thus, we generate pulses of fixed duration and random amplitude.

Let us designate the value of $z(t)$ at each sampling instant by A_i where i designates the sampling time. This value, A_i, is held for the entire period of the output. A_i is, of course, a random variable and we desire to measure its variance; i.e.,

$$\text{var}(A) = \lim_{N\to\infty} \frac{1}{N} \sum_{i=1}^{N} (A_i - \bar{A})^2 \quad \text{where} \quad \bar{A} = \lim_{N\to\infty} \frac{1}{N} \sum_{i=1}^{N} A_i \tag{3-1}$$

Following well-known methods [1, 2], we can easily find the power spectrum of the output of the sample and hold circuit.

$$p(\omega) = \frac{4\,\text{var}(A)}{T} \quad \frac{\sin^2 \frac{\omega T}{2}}{\omega^2} + \bar{A}^2 \delta(\omega) \tag{3-2}$$

where $T = 1$ m sec in our system.

Suppose now that we put this waveform into an RMS meter. What does the meter measure? First of all, the delta function is rejected since the meter being used rejects zero frequency. Thus, the meter measures the following:

$$\text{RMS} = \sqrt{\frac{1}{2\pi} \int_{\omega \neq 0} p(\omega)\, d\omega} = \sqrt{\frac{4\,\text{var}(A)}{2\pi T} \int_{-\infty}^{\infty} \frac{\sin^2 \frac{\omega T}{2}}{\omega^2}\, d\omega} \tag{3-3}$$

The integral is a tabulated one and equals $\pi T/2$.

$$\therefore \text{RMS} = \sqrt{\frac{4\,\text{var}(A)}{2\pi T} \frac{\pi T}{2}} = \sqrt{\text{var}(A)} \tag{3-4}$$

Thus, we read exactly what we wish since var(A) is the variance of the sample amplitudes. Since the sample and hold operation may be done at any point in time, the variance can be measured as a function of time.

The accuracy of the variance circuit can be easily checked by the ergodic theorem. If a stationary, zero mean noise voltage is applied to the RMS meter, the time average of the variance is measured. If the same noise voltage is passed through the sample and hold circuit and then applied to the RMS meter, then the ensemble average of the variance is measured. By ergodicity, these two measurements must be equal. The sample and hold measurement is always low by 2-3%. Taking this into account, the error in the variance measurement can be made very small.

It may be noted that the sample and hold waveform has the same statistics as the samples. Thus, we may perform further measurements on it to obtain, for example, higher moments.

IV. THEORETICAL AND EXPERIMENTAL RESULTS FOR THE MEAN

It is possible to derive some analytical results concerning the behavior of the mean. Consider the following system:

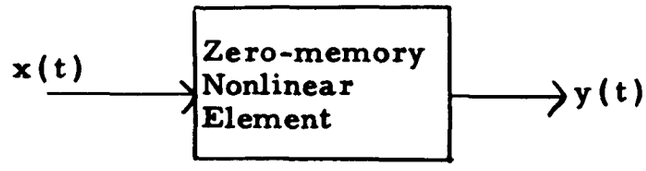

FIG. 7 Nonlinear Element

Assuming $x(t)$ to be the output of a narrow-band filter centered at frequency f_o, we can express $x(t)$ as follows:

$$x(t) = E(t)\cos[2\pi f_o t + a(t)] \tag{4-1}$$

$E(t)$ is the random envelope and $a(t)$ the random phase of $x(t)$. We represent the nonlinear operation as follows:

$$y = f(x) \tag{4-2}$$

or

$$y = f(E\cos\theta) \quad \text{where} \quad \theta = 2\pi f_o t + a \tag{4-3}$$

Following a currently popular technique [6, 7], we expand y into a Fourier cosine series since y is an even periodic function of θ.

$$\therefore y = \frac{1}{2} a_o + a_1 \cos\theta + a_2 \cos 2\theta + \ldots \tag{4-4}$$

and

$$a_n = \frac{1}{\pi} \int_0^{2\pi} f(E\cos\theta)\cos n\theta \, d\theta \tag{4-5}$$

We are interested in the a_o term in y since the output is terminated by a low-pass filter.

Consider now a specific nonlinearity, namely, a half-wave linear element. This device is specified as follows:

$$\begin{aligned} f(E\cos\theta) &= E\cos\theta, \quad E\cos\theta \geq 0 \\ f(E\cos\theta) &= 0, \quad E\cos\theta < 0 \end{aligned} \tag{4-6}$$

and, of course, $E(t) \geq 0$.

$$a_o = \frac{2}{\pi} \int_0^{\pi/2} E \cos\theta \, d\theta = \frac{2E}{\pi} \tag{4-7}$$

$$\therefore y(t) = \frac{E(t)}{\pi} \quad \text{(Ignoring high-frequency terms)} \tag{4-8}$$

$$\overline{y(t)} = \frac{\overline{E(t)}}{\pi} \tag{4-9}$$

where the overbar indicates statistical averaging.

If the input noise to the narrow-band filter is Gaussian, then $E(t)$ is known to have a Rayleigh distribution in the presence of noise only. In the presence of sine-wave plus Gaussian noise, $E(t)$ is known to have a modified Rayleigh distribution. The means for both situations are known.

In the absence of sine-wave:

$$\overline{E(t)} = \overline{E}_n = \sqrt{\frac{\pi}{2}}\,\sigma \tag{4-10}$$

In the presence of sine-wave:

$$\overline{E(t)} = \overline{E}_{s+n} = \sqrt{\frac{\pi}{2}}\,\sigma e^{-\frac{A^2}{4\sigma^2}} \left[\left(1 + \frac{A^2}{2\sigma^2}\right) I_o\left(\frac{A^2}{4\sigma^2}\right) + \frac{A^2}{2\sigma^2} I_1\left(\frac{A^2}{4\sigma^2}\right)\right] \tag{4-11}$$

where A is the amplitude of the input sine-wave and σ is the RMS noise power at the input of the nonlinearity. I_o and I_1 are modified Bessel functions of orders zero and one, respectively

$$\therefore \overline{y_n(t)} = \frac{\sigma}{\sqrt{2\pi}} \tag{4-12}$$

and

$$\overline{y_{s+n}(t)} = \frac{\sigma}{\sqrt{2\pi}} e^{-\frac{A^2}{4\sigma^2}} \left[\left(1+\frac{A^2}{2\sigma^2}\right) I_o\left(\frac{A^2}{4\sigma^2}\right) + \frac{A^2}{2\sigma^2} I_1\left(\frac{A^2}{4\sigma^2}\right)\right] \quad (4\text{-}13)$$

At this point, it is convenient to define a signal-to-noise ratio. Let $\rho = A^2/2\sigma^2$. This gives the ratio of the mean square of the sine-wave to the mean square of the noise. Therefore,

$$\overline{y_{s+n}(t)} = \frac{\sigma}{\sqrt{2\pi}} e^{-\frac{\rho}{2}} \left[(1+\rho) I_o\left(\frac{\rho}{2}\right) + \rho I_1\left(\frac{\rho}{2}\right)\right] \quad (4\text{-}14)$$

In our experimental apparatus, the time interval during which the sine-wave is on is small compared to the period of the signal (100 μsec vs. 1 m sec). On a time average basis, therefore, the mean is very nearly $\overline{y_n(t)}$. However, the low-pass filter does not transmit zero frequency, and so the mean at the filter output is the response of the filter to the difference of the mean with and without signal. The following diagrams illustrate this behavior.

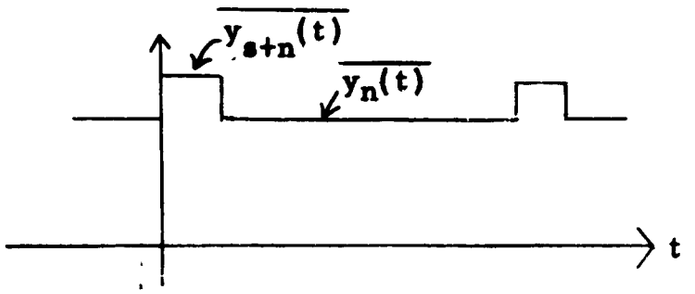

FIG. 8 Mean of y(t) Ignoring High-Frequency Terms

Subtracting out the time average of the mean, we obtain:

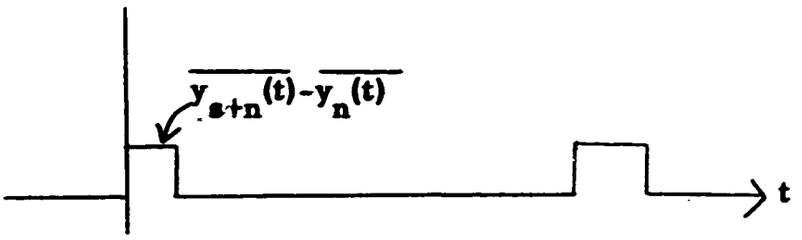

FIG. 9 Waveform of FIG. 8 Minus $\overline{y_n(t)}$

Let the output of the low-pass filter be $z(t)$. Therefore,

$$z(t) = \int_{-\infty}^{\infty} y(\tau)\, h(t-\tau)\, d\tau \tag{4-15}$$

and

$$\overline{z(t)} = \int_{-\infty}^{\infty} \overline{y(\tau)}\, h(t-\tau)\, d\tau \tag{4-16}$$

where

$$\overline{y(\tau)} = \overline{y_{s+n}(\tau)} - \overline{y_n(\tau)} \tag{4-17}$$

An interesting behavior of the mean for a half-wave linear element can now be demonstrated.

$$\overline{y(\tau)} = \frac{\sigma}{\sqrt{2\pi}}\, e^{-\frac{\rho}{2}} \left[(1+\rho)\, I_o\left(\frac{\rho}{2}\right) + \rho\, I_1\left(\frac{\rho}{2}\right)\right] - \frac{\sigma}{\sqrt{2\pi}} \tag{4-18}$$

Suppose now that $\rho \to \infty$, i.e., $\sigma \to 0$. Using the asymptotic behavior of the modified Bessel functions I_o and I_1, it can be easily shown that $\overline{y(\tau)} \to \frac{A}{\pi}$. If this pulse is the input mean to the low-pass filter, then we call the output mean the mean without noise. Further, $\overline{y(\tau)}$ is monotonic in ρ. Therefore, if we fix A and σ is either zero or some non-zero constant, then $\overline{y(\tau)}$ with noise ($\sigma \neq 0$) is less than $\overline{y(\tau)}$ without noise ($\sigma = 0$). This is a sufficient condition to prove that the mean, $\overline{z(t)}$, at the output of the low-pass filter is always suppressed in the presence of noise. If $\overline{z_s(t)}$ is the output mean in the absence of noise and $\overline{z_{s+n}(t)}$ is the output mean in the presence of noise, then the following is true:

$$|\overline{z_{s+n}(t)}| \leq |\overline{z_s(t)}| \tag{4-19}$$

and furthermore, $\overline{z_{s+n}(t)} = K\overline{z_s(t)}$ where K is less than one and can be calculated as a function of ρ.

In Figs. 14a, b at the end of this report, experimental curves are shown demonstrating this effect along with experimental and calculated values for K, the suppression factor. The low-pass filter has been set to give considerable filtering of the signal envelope. Pre-detection 3 dB bandwidth is 15 Kc and low-pass 3 dB bandwidth is 8 Kc.

Let us now consider the case where the nonlinear element is a half-wave square-law device. In this case,

$$\begin{aligned} f(E\cos\theta) &= E^2\cos^2\theta, \quad E\cos\theta \geq 0 \\ f(E\cos\theta) &= 0, \quad E\cos\theta < 0 \end{aligned} \tag{4-20}$$

Proceeding as before, we find

$$a_o = \frac{1}{2} E^2 \tag{4-21}$$

and

$$y(t) = \frac{1}{4} E^2(t) \text{ (Ignoring high-frequency terms)} \tag{4-22}$$

In the absence of sine-wave:

$$\overline{y_n(t)} = \frac{1}{4} \overline{E_n^2(t)} = \frac{\sigma^2}{2} \tag{4-23}$$

In the presence of sine-wave:

$$\overline{y_{s+n}(t)} = \frac{1}{4} \overline{E_{s+n}^2(t)} = \frac{1}{4} (A^2 + 2\sigma^2) \tag{4-24}$$

and

$$\overline{y_{s+n}(t)} - \overline{y_n(t)} = \frac{A^2}{4} \tag{4-25}$$

This leads to an interesting result since the above is independent of the noise. Thus, the output mean is the same both with and without noise, i.e.,

$$\overline{z_{s+n}(t)} = \overline{z_s(t)}$$

In Fig. 15 at the end of this report, experimental curves are shown demonstrating the above result.

Now suppose that a half-wave linear with clipping characteristic is used as follows:

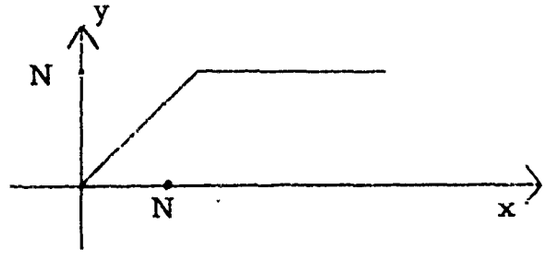

FIG. 10 Half-wave Linear Characteristic with Clipping

Proceeding as before, we find

$$y(t) = \frac{1}{\pi} E(t), \quad 0 \leq E(t) \leq N$$

$$y(t) = \frac{N}{\pi}, \quad E(t) \geq N$$

The density functions of $E(t)$ with and without signal appear as follows

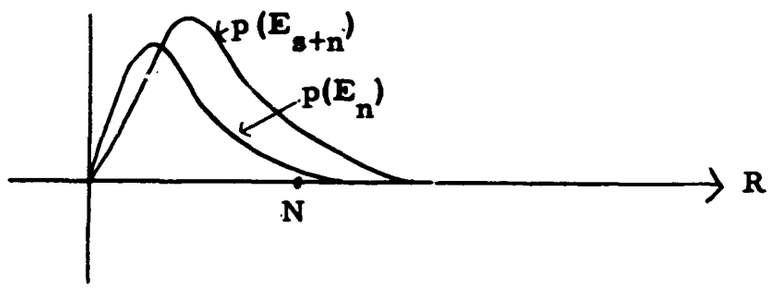

FIG. 11 Density Functions of $E(t)$ With and Without Signal

Inspection of this diagram shows that $\overline{E}_{s+n} - \overline{E}_n$ is less now than when the clipper is absent although the amount cannot be calculated exactly. This indicates additional suppression of the mean with the addition of the clipper.

In Figs. 14a,b data showing this effect are given. The clipper passes signal without noise unchanged. Therefore, the curves of mean without noise are identical to those for the half-wave linear device. The mean with noise, however, is somewhat further suppressed below that of the unclipped detector.

It should be pointed out that the dc rejection of the low-pass filter does not produce the above effects but instead displays them. The important point is that the time-varying response of the mean behaves as shown regardless of any dc values that may or may not be present.

V. THEORETICAL AND EXPERIMENTAL RESULTS FOR THE VARIANCE

In the presence of a burst of sine-wave, the output of the nonlinear element, $y(t)$, (cf. Fig. 2) has a non-stationary auto-correlation function which we designate as $R_y(t_1, t_2)$. However, if we concern ourselves with the low-frequency part of $y(t)$, namely $E(t)$ or some power or modified version of it, then $E(t)$ is a stationary process for noise alone as input or for sine-wave plus noise as input. Thus, the low-frequency output is, so to speak, "piecewise" stationary. The following diagram of the t_1, t_2 plane shows the behavior of the low-frequency auto-correlation function as we switch from noise to signal plus noise.

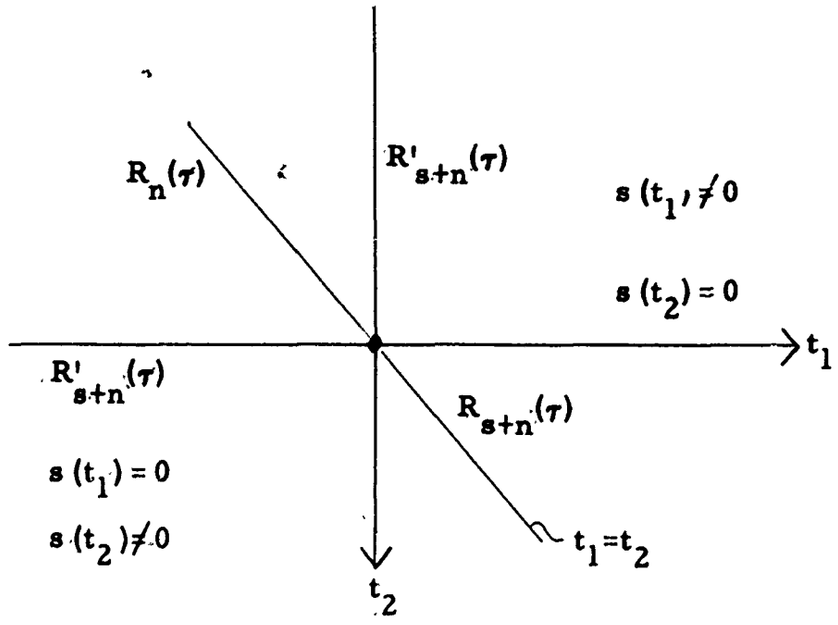

FIG. 12 Diagram Pertaining to a Comparison of $R_y(t_1, t_2)$ With and Without Signal

Sine-wave is turned on at $t_1 = t_2 = 0$. $R'_{s+n}(\tau)$ designates that $s(t_1) \neq 0$, $s(t_2) = 0$, or vice-versa. This behavior occurs in the first and third quadrants. $R_y(t_1, t_2)$ is stationary in each quadrant of the t_1, t_2 plane, i.e., $R_y(t_1, t_2) = R_y(\tau)$ where $\tau = t_2 - t_1$. We can express the variance at the output of the low-pass filter as follows:

$$\text{var}\left\{z(t)\right\} = \int_{-\infty}^{\infty}\int_{-\infty}^{\infty} R_y(t_1, t_2)\, h(t-t_1)\, h(t-t_2)\, dt_1\, dt_2 \qquad (5\text{-}1)$$

In problems of this sort, it can be shown that the auto-correlation function can be written in a series [2], the first term of which produces the squared mean at the low-pass output. In what follows, we assume that this term has been subtracted out, so that the above gives the variance and not the mean square of the output.

We can rewrite Eq. (5-1) as follows:

$$\text{var}\left\{z(t)\right\} = \int_{-\infty}^{\infty}\int_{-\infty}^{\infty} R_n(\tau)\, h(t-t_1)\, h(t-t_2)\, dt_1\, dt_2 + \int_{0}^{\infty}\int_{0}^{\infty} [R_{s+n}(\tau) - R_n(\tau)]\, h(t-t_1) h(t-t_2) dt_1 dt_2$$

$$- 2\int_{0}^{\infty}\int_{-\infty}^{0} R'_{s+n}(\tau)\, h(t-t_1)\, h(t-t_2)\, dt_1\, dt_2 \qquad (5\text{-}2)$$

The first term may be rewritten as

$$\int_{-\infty}^{\infty} P_n(\omega)\, |H(\omega)|^2\, d\omega \qquad (5\text{-}3)$$

where $P_n(\omega)$ and $H(\omega)$ are the Fourier transforms of $R_n(\tau)$ and $h(\tau)$, respectively. This term is recognized as the steady-state response of the variance at the low-pass output when only noise is present in the system.

The second term may be written as

$$\int_{-\infty}^{\infty} [P_{s+n}(\omega) - P_n(\omega)] \; |H(\omega, t)|^2 \, d\omega \tag{5-4}$$

where

$$H(\omega, t) = \int_{o}^{t} h(x) \, e^{-j\omega x} \, dx \tag{5-5}$$

This term is a function of time as is the third term.

For $t \leq 0$, the variance is given by the following

$$\text{var}\left\{z(t)\right\} = \int_{-\infty}^{\infty} P_n(\omega) \, |H(\omega)|^2 \, d\omega \tag{5-6}$$

This is the stationary variance of the $n(t)$ process at the output of the low-pass filter assuming that $n(t)$ has existed at the input for a time interval greater than the memory of the low-pass filter.

As $t \to \infty$, assuming that the $s(t) + n(t)$ process is left on for a time greater than the memory of the low-pass filter, the variance is given by the following

$$\text{var}\left\{z(t)\right\} = \int_{-\infty}^{\infty} P_{s+n}(\omega) \, |H(\omega)|^2 \, d\omega \tag{5-7}$$

This is the stationary variance of the $s(t) + n(t)$ process at the output of the low-pass filter.

The low-frequency variance at the output of the half-wave nonlinear element will, in general, have the following form

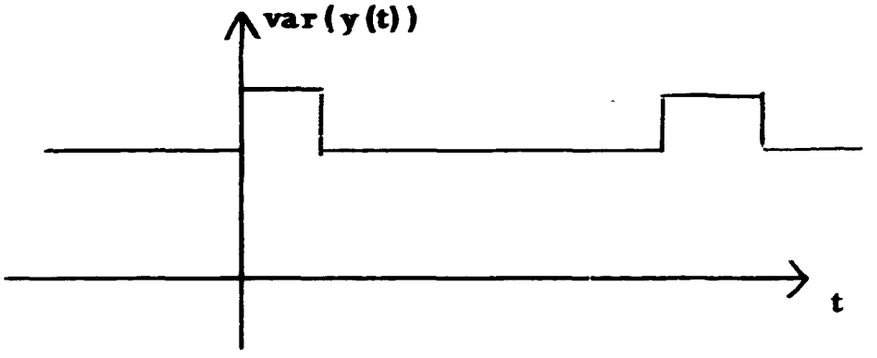

FIG. 13 Variance of $y(t)$ Ignoring High-Frequency Terms

If the low-pass filter had sufficiently wide bandwidth, then the output variance would have the same form as above, i.e., the low-pass filter would completely pass the low-frequency spectrum. However, if the low-frequency spectrum is filtered, then this form will not be preserved. Experimental data for the variance are shown in Fig. 16 for the half-wave linear element. If only noise is present at the input, then the output variance is given by Eq. (5-6) and is shown experimentally by the line labeled "noise alone." If the signal were left on indefinitely, i.e., the input is sine-wave plus noise, then the output variance would be a constant given by Eq. (5-7) and is shown experimentally by the line labeled "sine-wave plus noise." Thus, the non-stationary variance is seen to equal the value given by Eq. (5-6) before the

signal burst occurs and then increases toward the value given by Eq. (5-7) when the signal burst is applied. Then, when the signal is turned off, the variance returns to the value given by Eq. (5-6).

If the signal burst were left on for a sufficient length of time, then we would expect the non-stationary variance to attain the value given by Eq. (5-7). That this actually occurs is shown in Fig. 17 where the burst was left on for a longer time but all other parameters were unchanged.

In Figs. 18 and 19 are shown the variance curves for the half-wave linear with clipping and half-wave square law devices. The clipper reduces the variance, as expected, and the half-wave square law device exhibits a very pronounced increase in the variance during the time-varying response.

VI. THE MEAN SQUARE

A measurement of the mean square has not been considered necessary. The mean square of the output, $z(t)$, is given by the following:

$$\overline{z^2(t)} = \overline{z(t)}^2 + \text{var}\{z(t)\} \qquad (6\text{-}1)$$

Since the mean and the variance can be accurately measured, the mean square may be calculated. Experimental data on the mean square are given in Figs. 20, 21, 22. Since the squared mean is positive and the variance was not observed to go below its value for noise alone as input, it is seen that the output mean square is increased in the presence of signal. This can be used as a basis for detecting a signal.

VII. AMPLITUDE DISTRIBUTION FUNCTION

Purely theoretical results for the amplitude distribution function are difficult to obtain. This is the problem of passing a non-Gaussian process through a linear filter and calculating the output distribution function. This is an unsolved problem.

At this stage of our work, the amplitude distribution functions have been measured for the nonlinearities already mentioned. The envelope has a Rayleigh density but with filtering of the low-frequencies, the density is unknown.

Figures 23a, 23b and 24 show the measured amplitude distribution functions, or, to be exact, one minus the distribution function. At 180 μ sec delay with respect to the leading edge of the input pulse, the effect of the signal is not present and the distribution function of noise is measured. At 280 μ sec delay, the maximum of the output mean occurs. The distribution function is shifted to the right due to the change in the mean and also is seen to have an increased spread, indicating an increase in the variance. Both of these observations are consistent with the data for the mean and variance.

If Gaussian noise is passed through the system and a half-wave linear element is used, then we should obtain a Rayleigh density at the output if the low-pass bandwidth is sufficiently wide. If a half-wave square-law device is used, then an exponential density is expected. These distributions have been obtained and are shown in Figs. 25 and 26. Also shown here are plots

of $\ln\left[-\ln\left\{1-F(z)\right\}\right]$ vs. $\ln z$. For a Rayleigh distribution, this will give a straight line with slope 2.00. For an exponential distribution, it will give a straight line with slope 1.00. These data demonstrate that the system can produce known results.

VIII. OUTPUT SIGNAL-NOISE RATIO AND DETECTION CHARACTERISTICS

Signal-noise ratio is not a unique quantity but the following choice has been studied in this work:

$$SNR = \frac{\overline{z_{s+n}^2(t)} - \overline{z_n^2(t)}}{\overline{z_n^2(t)}} \quad . \tag{8-1}$$

$z_{s+n}(t)$ is the output when signal plus noise is applied at the input and $z_n(t)$ is the output when noise alone is present in the system. This choice of SNR thus gives a measure of the excess power in the output when signal is applied to the input. Curves in Figs. 27, 28, and 29 show the output SNR for three nonlinearities. The half-wave square-law device gives a higher SNR than the half-wave linear, and the presence of a clipper on the half-wave linear degrades the SNR.

From a detection point of view, SNR is not necessarily significant and the detection characteristic is of greater interest. This gives the probability of detection for a given false alarm probability and this data can be read directly from the amplitude distribution curves. Detection characteristics are given in Figs. 30 and 31. These curves show that

the half-wave square law and the half-wave linear devices are equivalent, and the half-wave linear device with clipping degrades the detection characteristic. This cannot be shown analytically, since the output distribution functions cannot be calculated. The above can be demonstrated analytically for strictly envelope detectors, however, for detecting signals of unknown phase [9].

IX. FUTURE WORK

The experimental system at present simulates detection plus low-pass integration. Other forms of integration will be examined, in particular, RC integration and ideal integration, i.e., unweighted integration. The effects of these forms of integration on signal-to-noise ratio and signal detectibility will be examined. The effect of different nonlinear elements will also be investigated.

An attempt to classify the distribution functions at the output of the low-pass filter and integrator will be made using the Pearson class of distributions and also series approximations in terms of moments. To this end, the third and fourth moments will be measured.

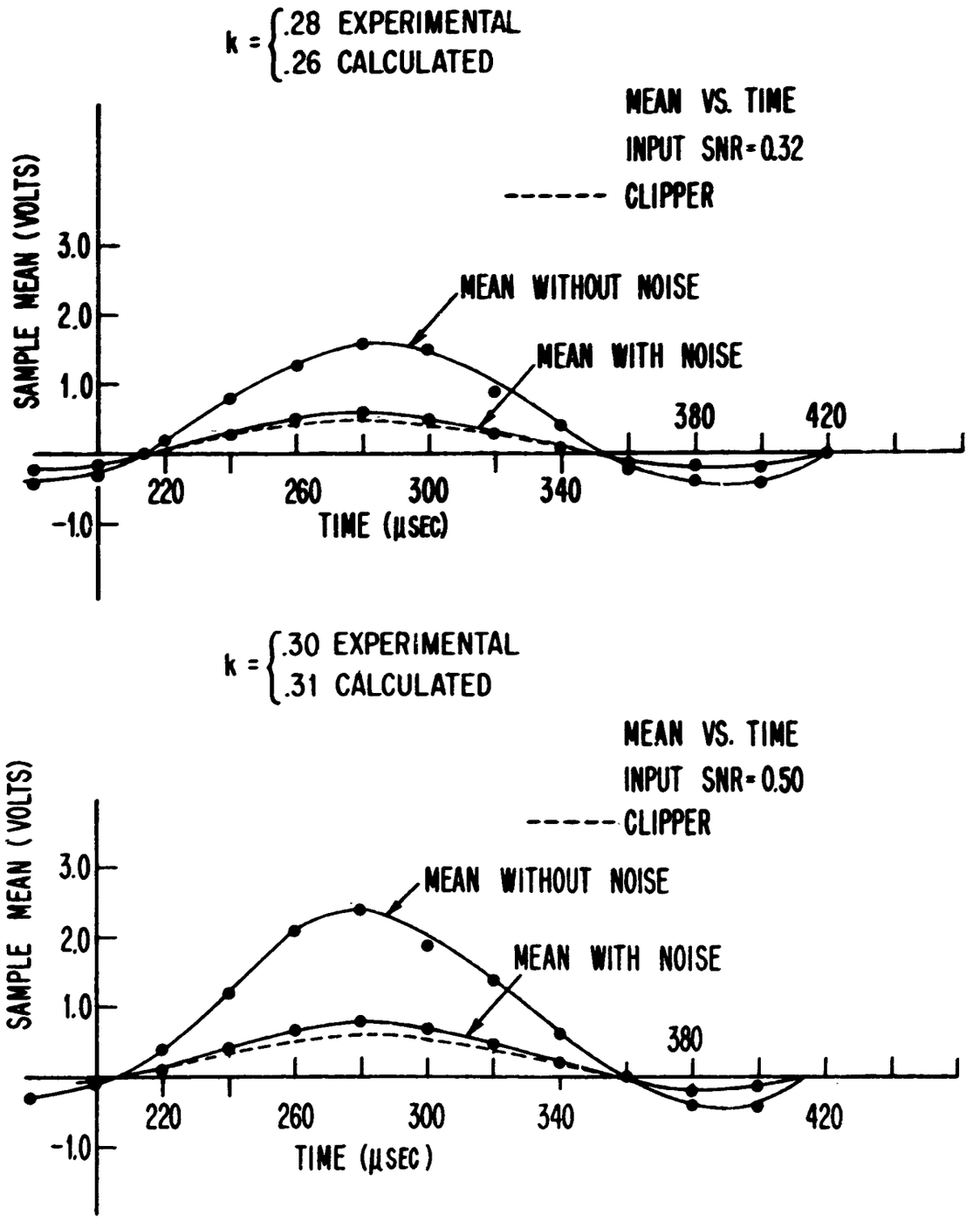

FIG. 14a MEAN RESPONSE FOR HALF-WAVE LINEAR DEVICE WITH AND WITHOUT CLIPPING WITH CONSTANT NOISE POWER (σ^2)

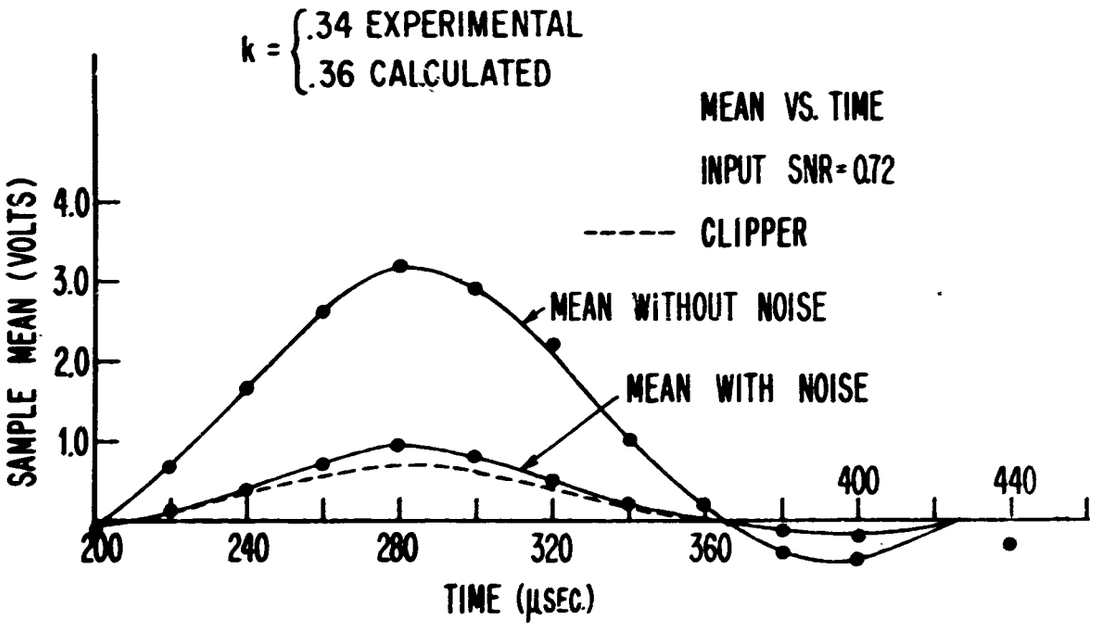

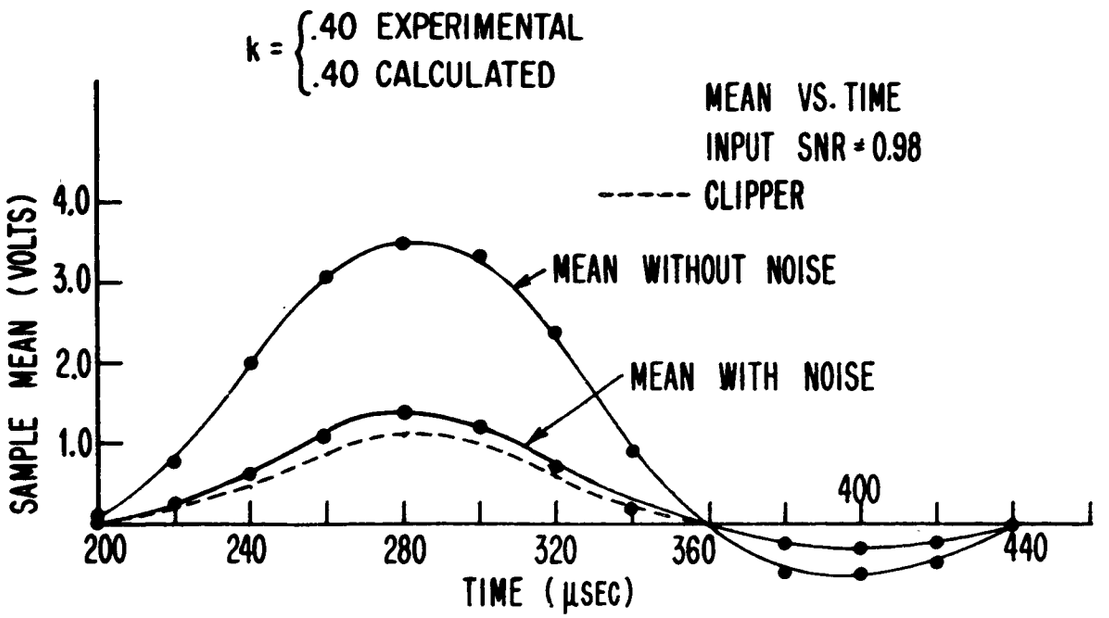

FIG. 14b MEAN RESPONSE FOR HALF-WAVE LINEAR DEVICE WITH AND WITHOUT CLIPPING WITH CONSTANT NOISE POWER (σ^2)

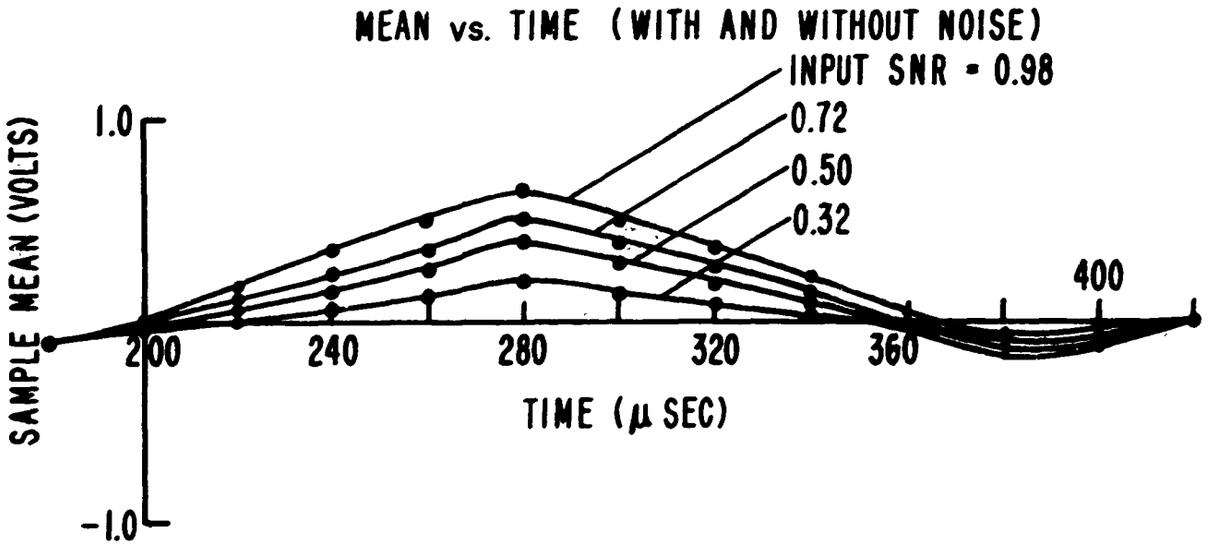

FIG. 15 MEAN FOR HALF-WAVE SQUARE LAW DEVICE WITH INPUT NOISE POWER CONSTANT

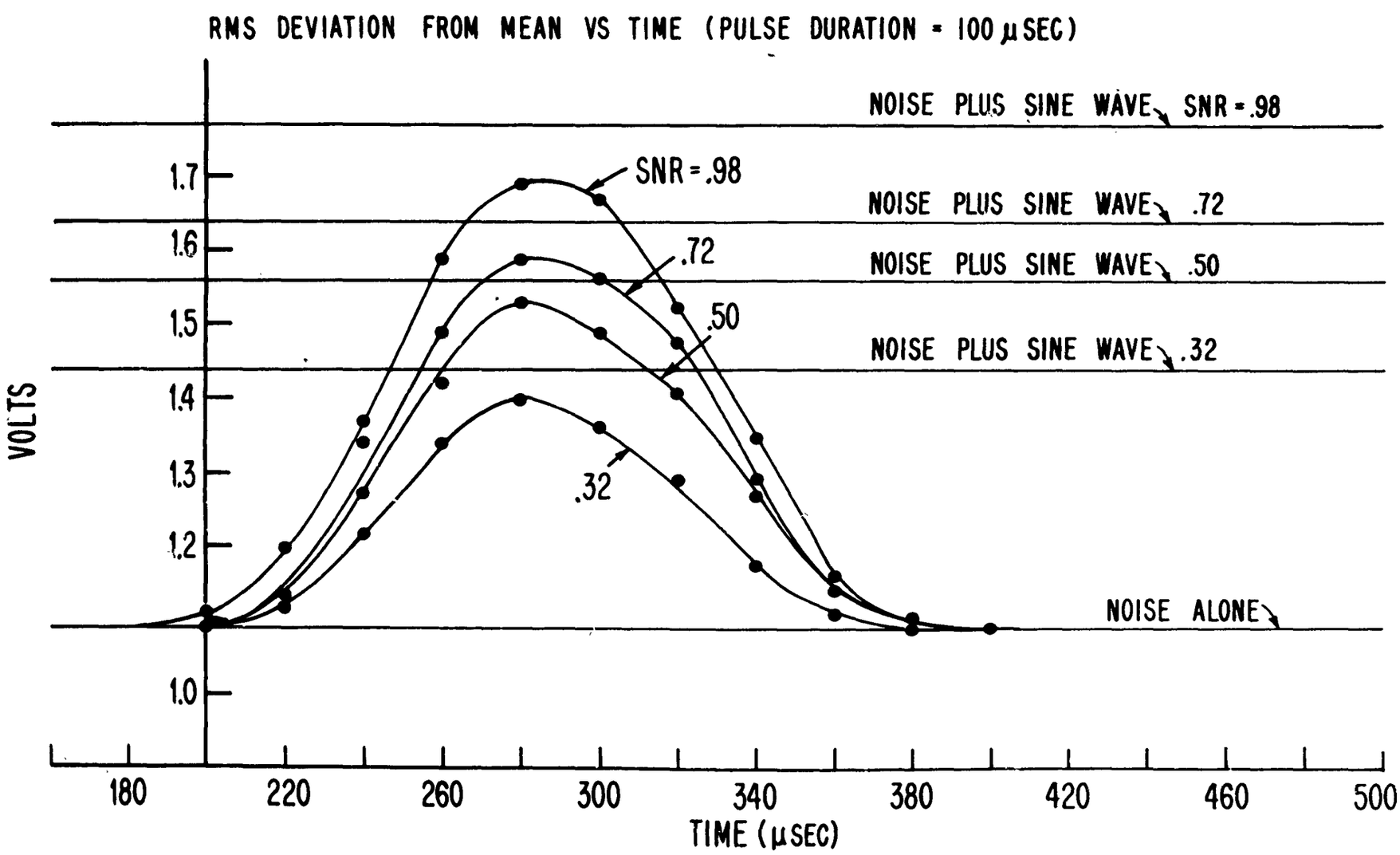

FIG. 16 SQUARE ROOT OF VARIANCE FOR HALF-WAVE LINEAR DEVICE WITH INPUT NOISE POWER CONSTANT (σ^2)

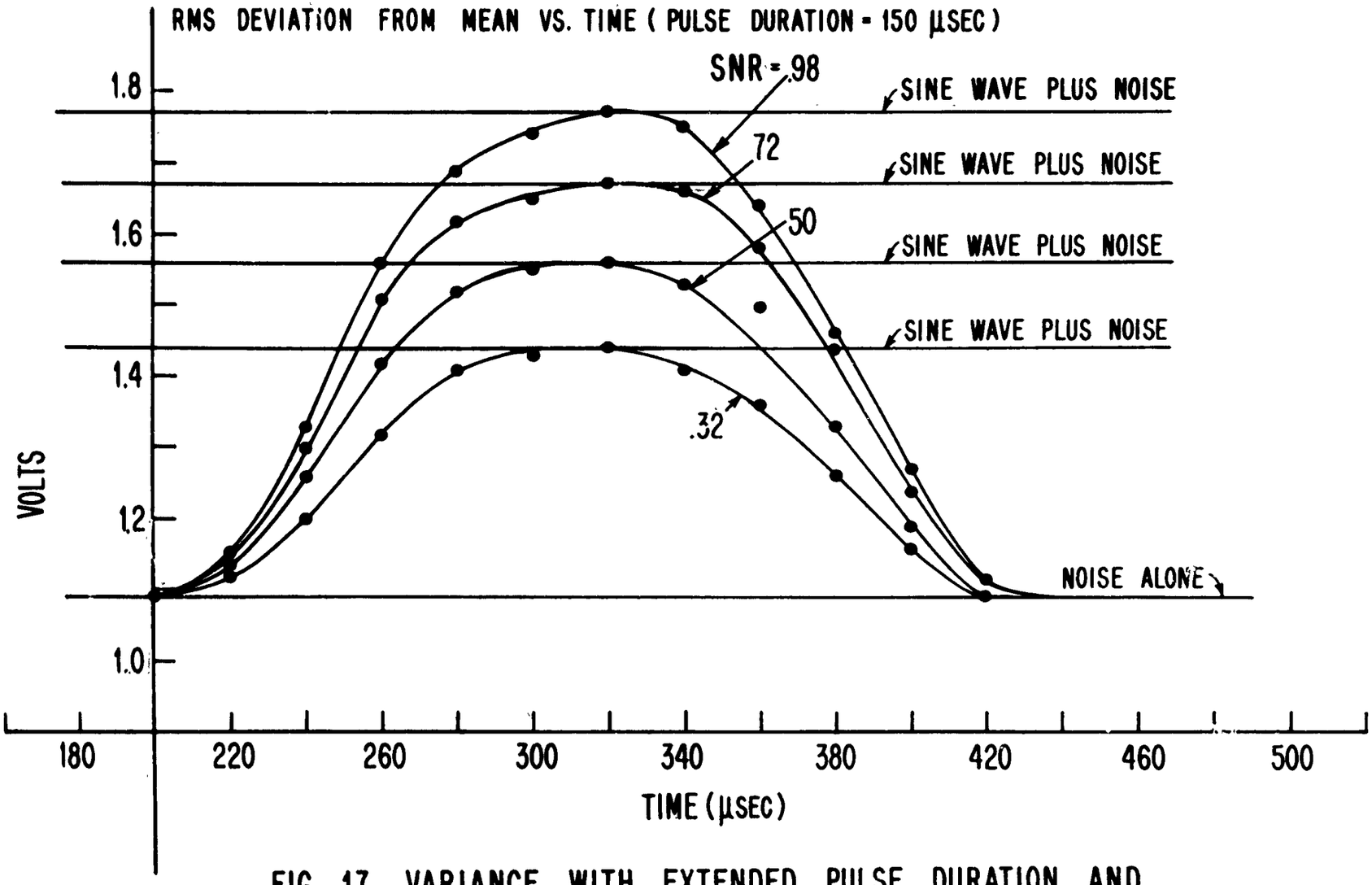

FIG. 17 VARIANCE WITH EXTENDED PULSE DURATION AND CONSTANT NOISE POWER (σ^2)

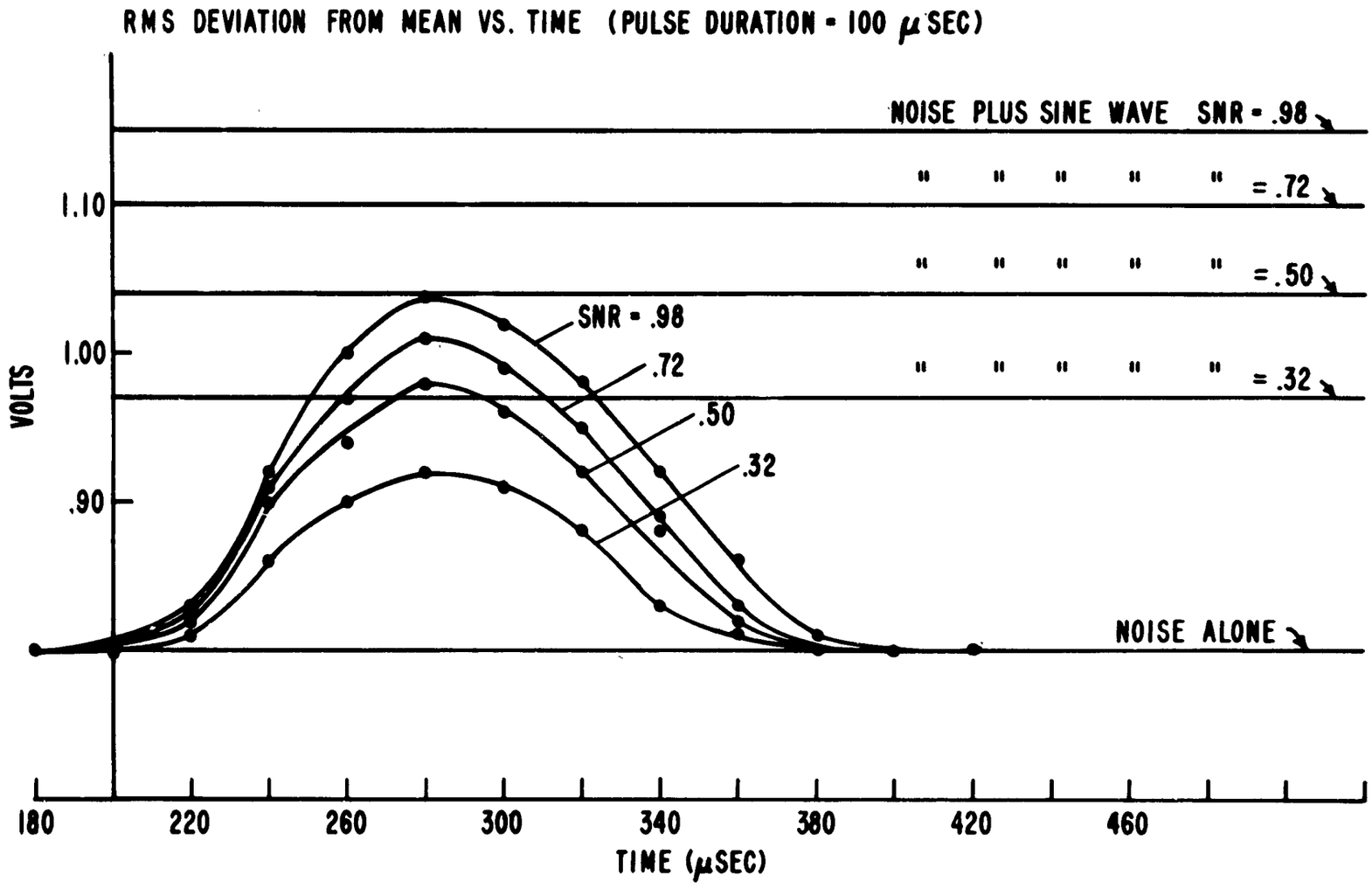

FIG. 18 SQUARE ROOT OF VARIANCE FOR HALF-WAVE LINEAR DEVICE WITH CLIPPING WITH INPUT NOISE POWER CONSTANT (σ^2)

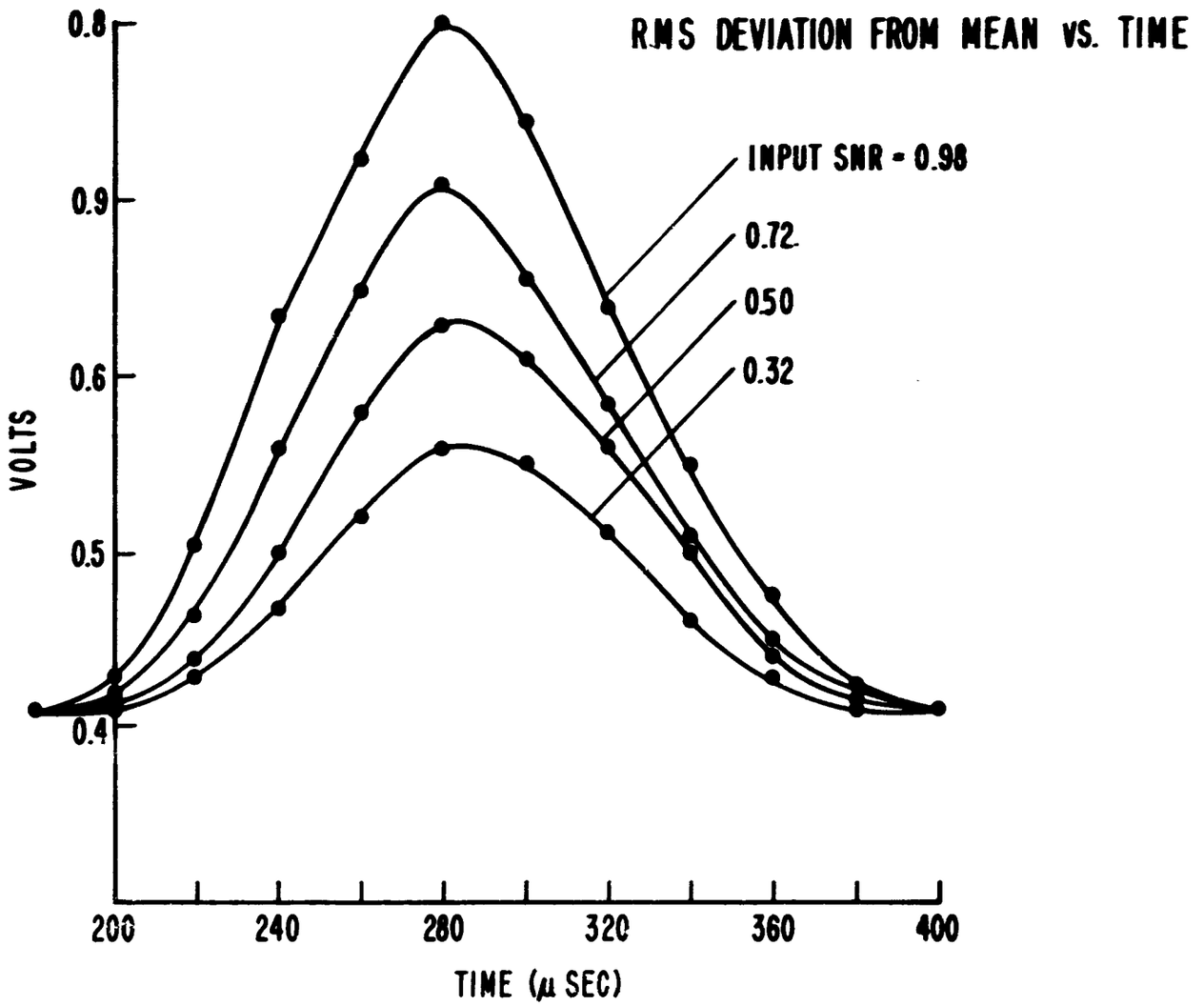

FIG. 19 SQUARE ROOT OF VARIANCE FOR HALF-WAVE SQUARE LAW DEVICE WITH INPUT NOISE POWER CONSTANT (σ^2)

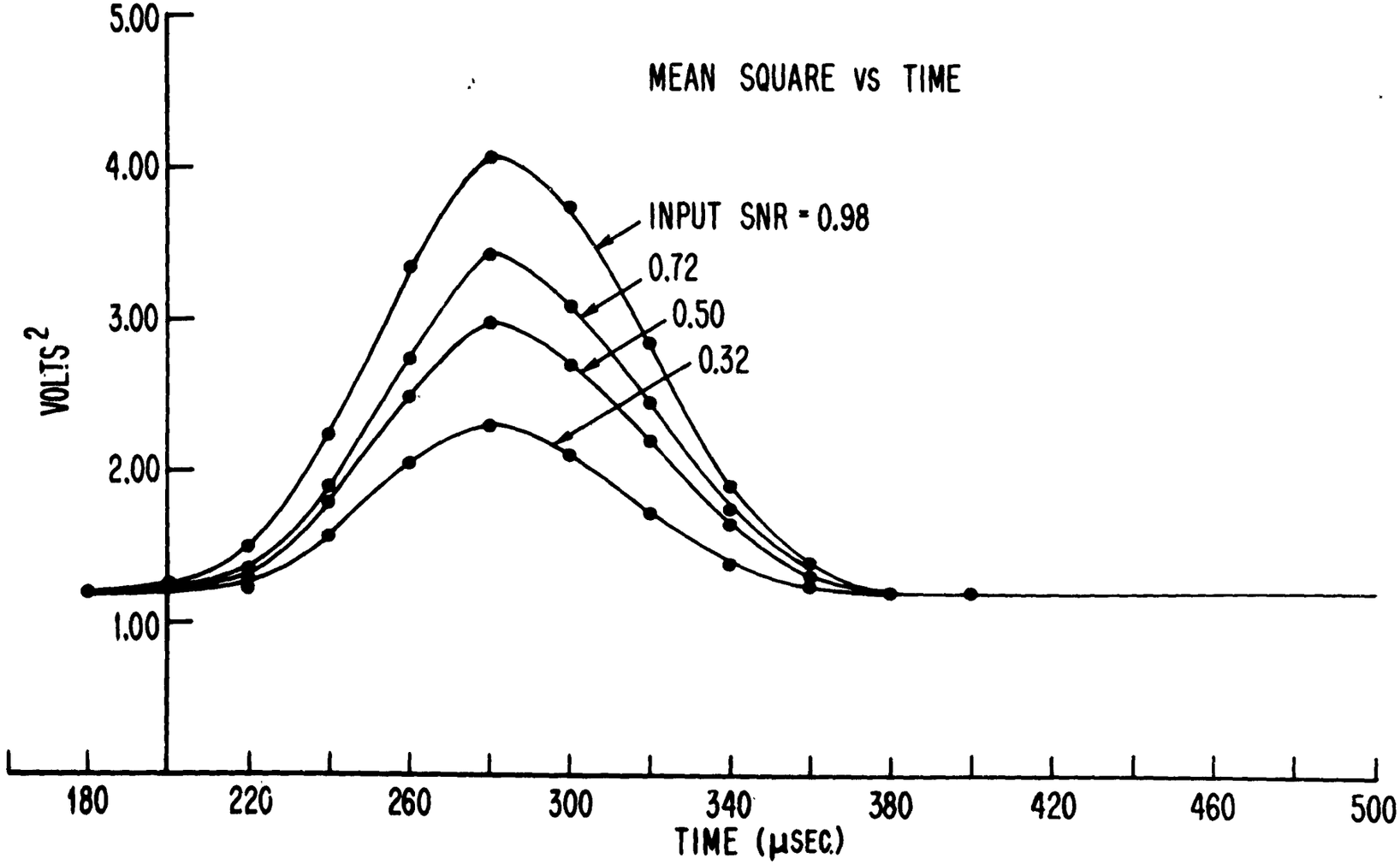

FIG. 20 MEAN SQUARE FOR HALF-WAVE LINEAR DEVICE WITH CONSTANT INPUT NOISE POWER (σ^2)

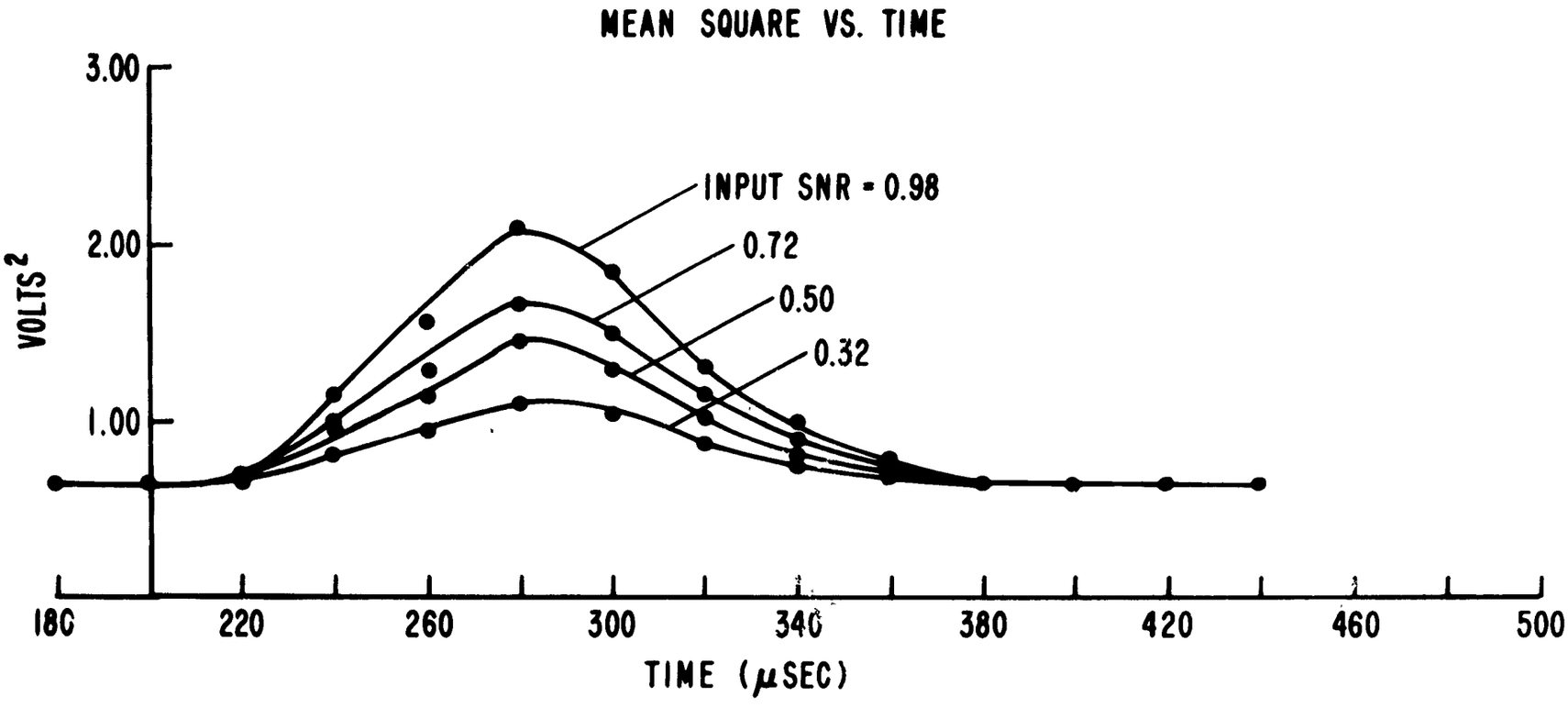

FIG. 21 MEAN SQUARE FOR HALF-WAVE LINEAR DEVICE WITH CLIPPING WITH CONSTANT INPUT NOISE POWER (σ^2)

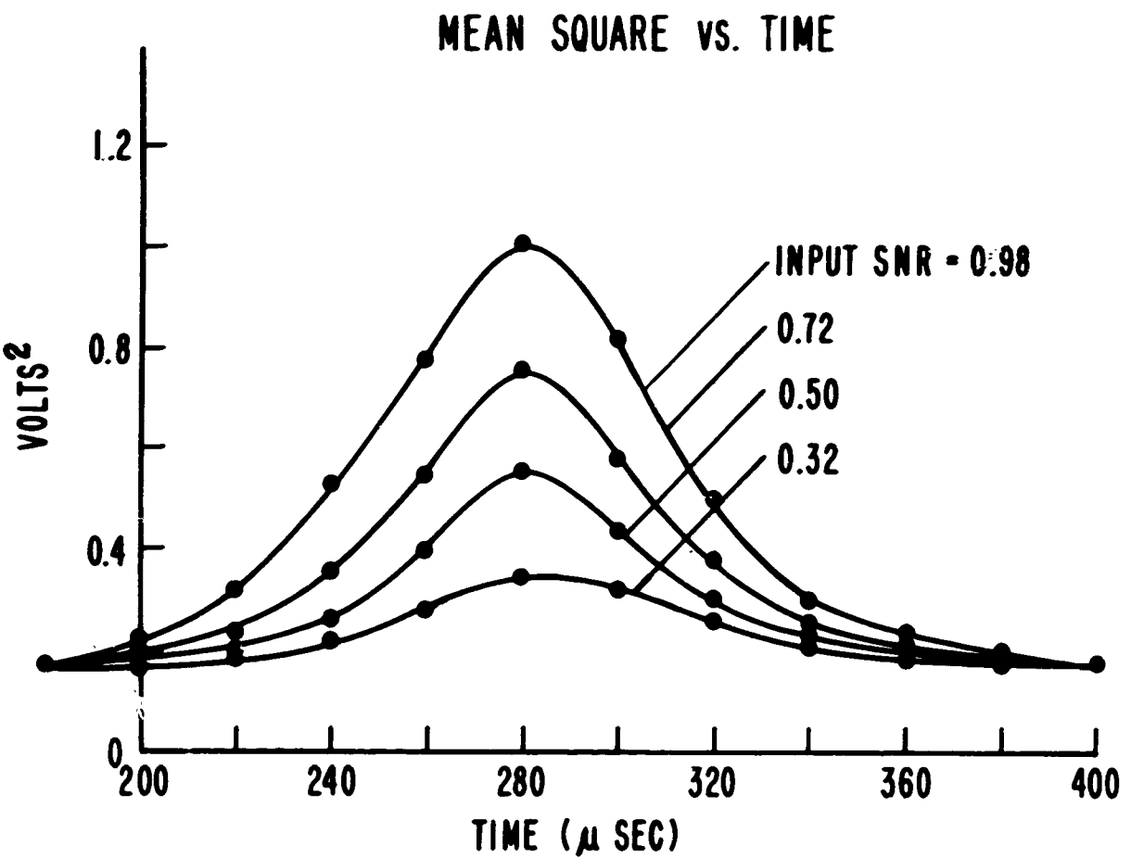

FIG. 22 MEAN SQUARE FOR HALF-WAVE SQUARE LAW DEVICE WITH CONSTANT INPUT NOISE POWER (σ^2)

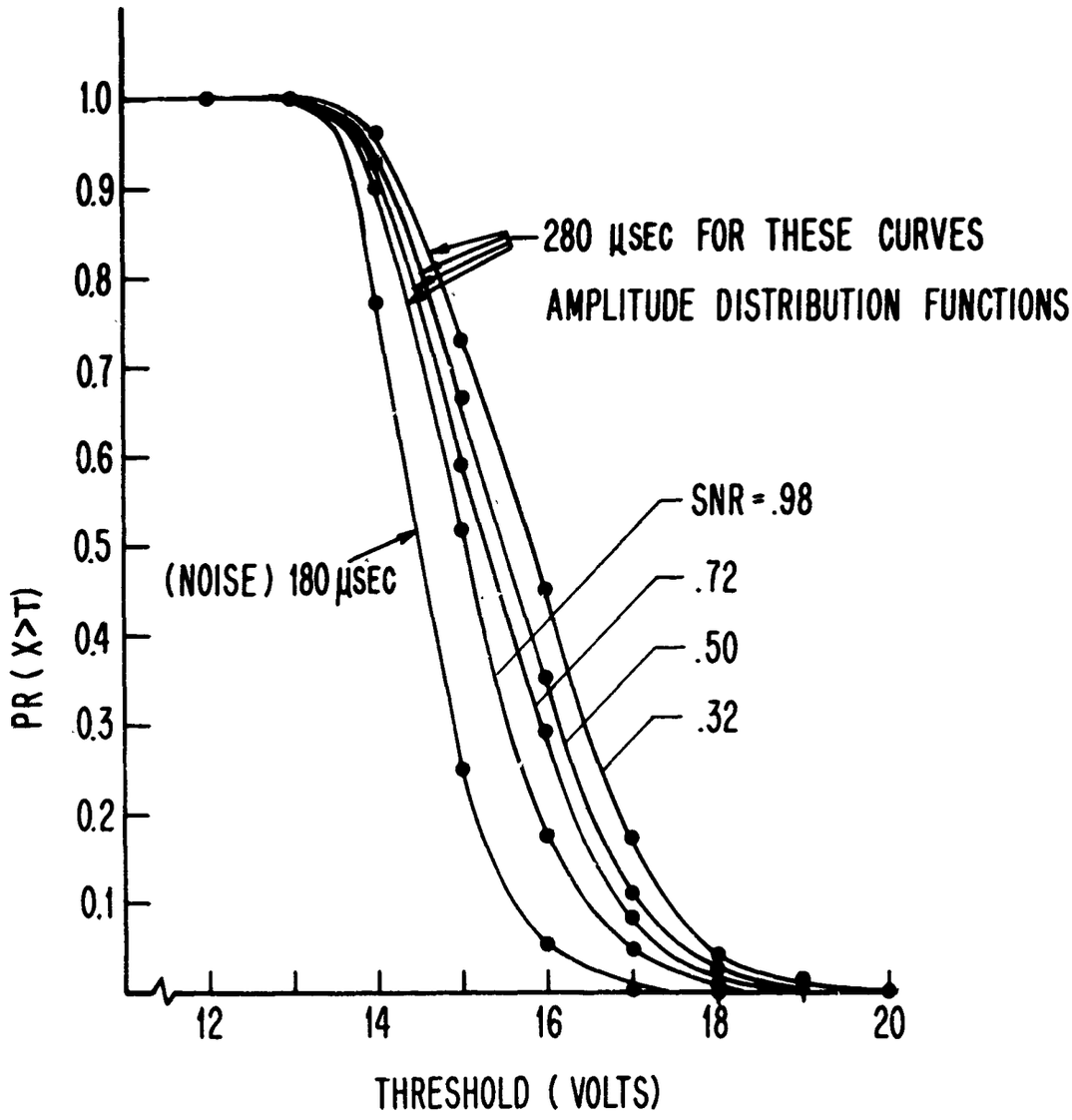

FIG. 23a AMPLITUDE DISTRIBUTION FUNCTION FOR HALF-WAVE LINEAR DEVICE.

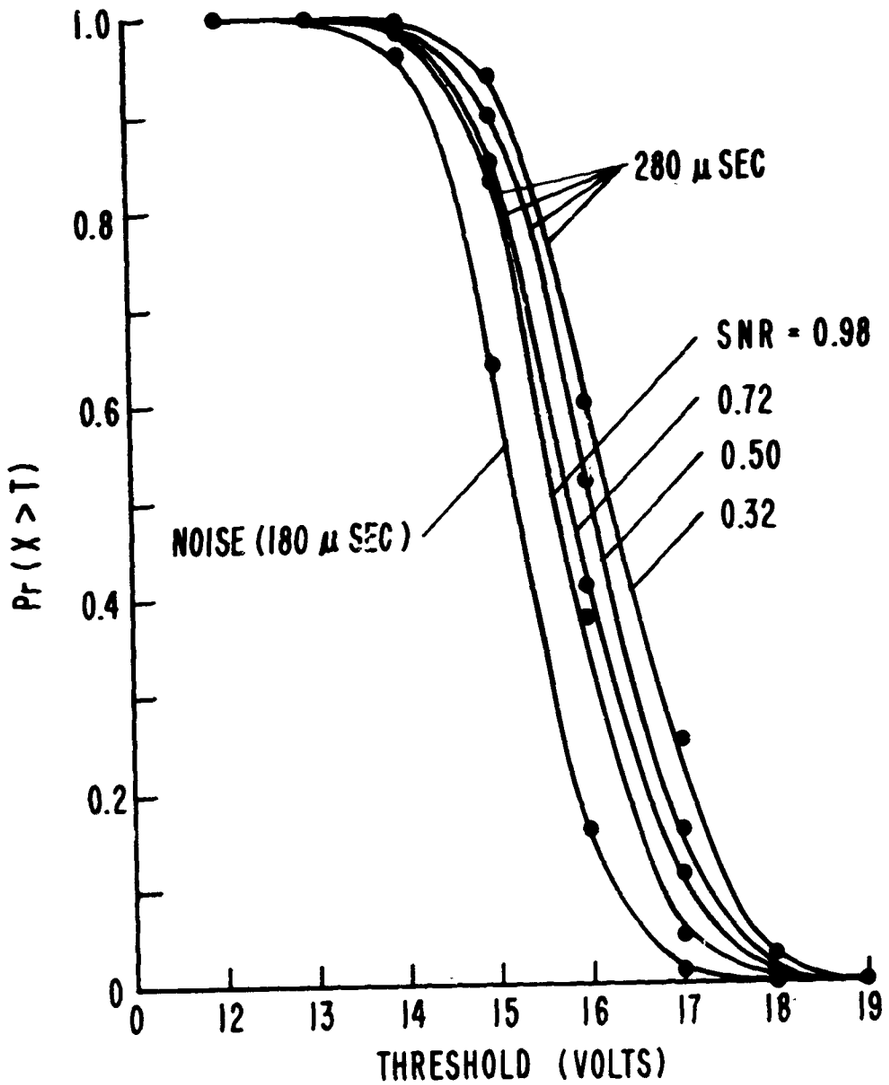

FIG. 23b AMPLITUDE DISTRIBUTION FUNCTION FOR HALF-WAVE LINEAR DEVICE WITH CLIPPING.

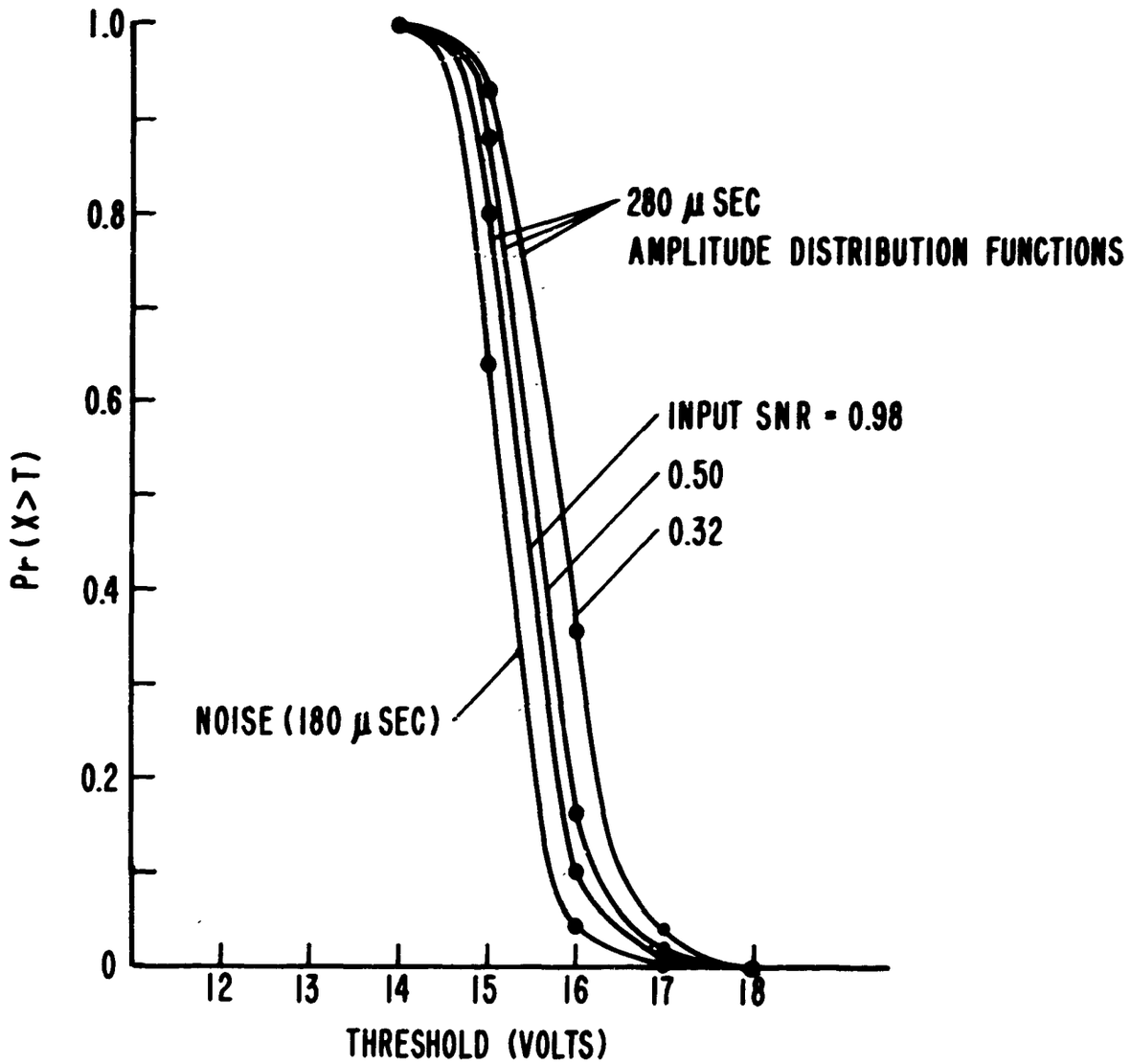

FIG. 24 AMPLITUDE DISTRIBUTION FUNCTION FOR HALF-WAVE SQUARE LAW DEVICE.

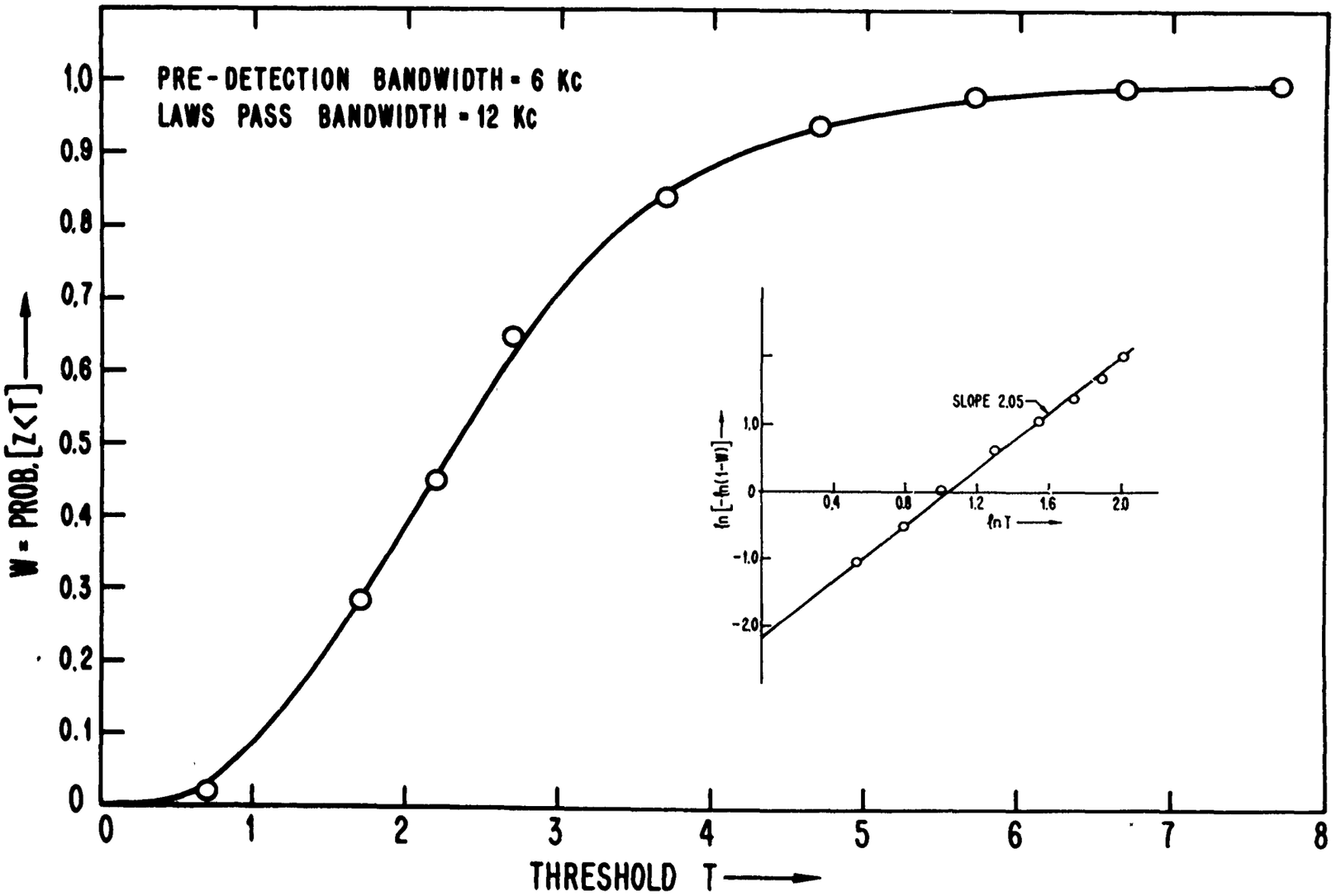

FIG. 25 EXPERIMENTAL RALEIGH DISTRIBUTION

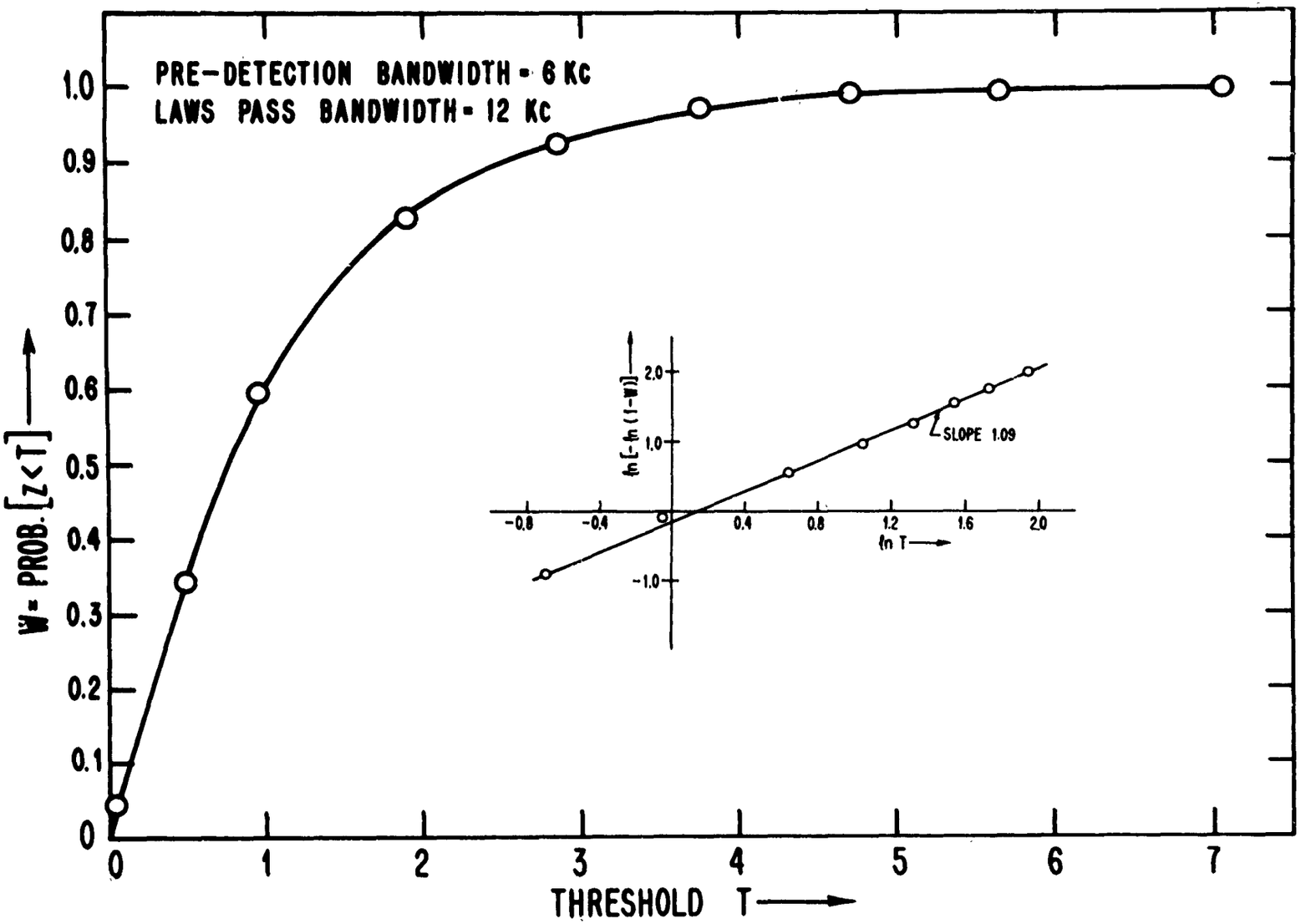

FIG. 26 EXPERIMENTAL EXPONENTIAL DISTRIBUTION

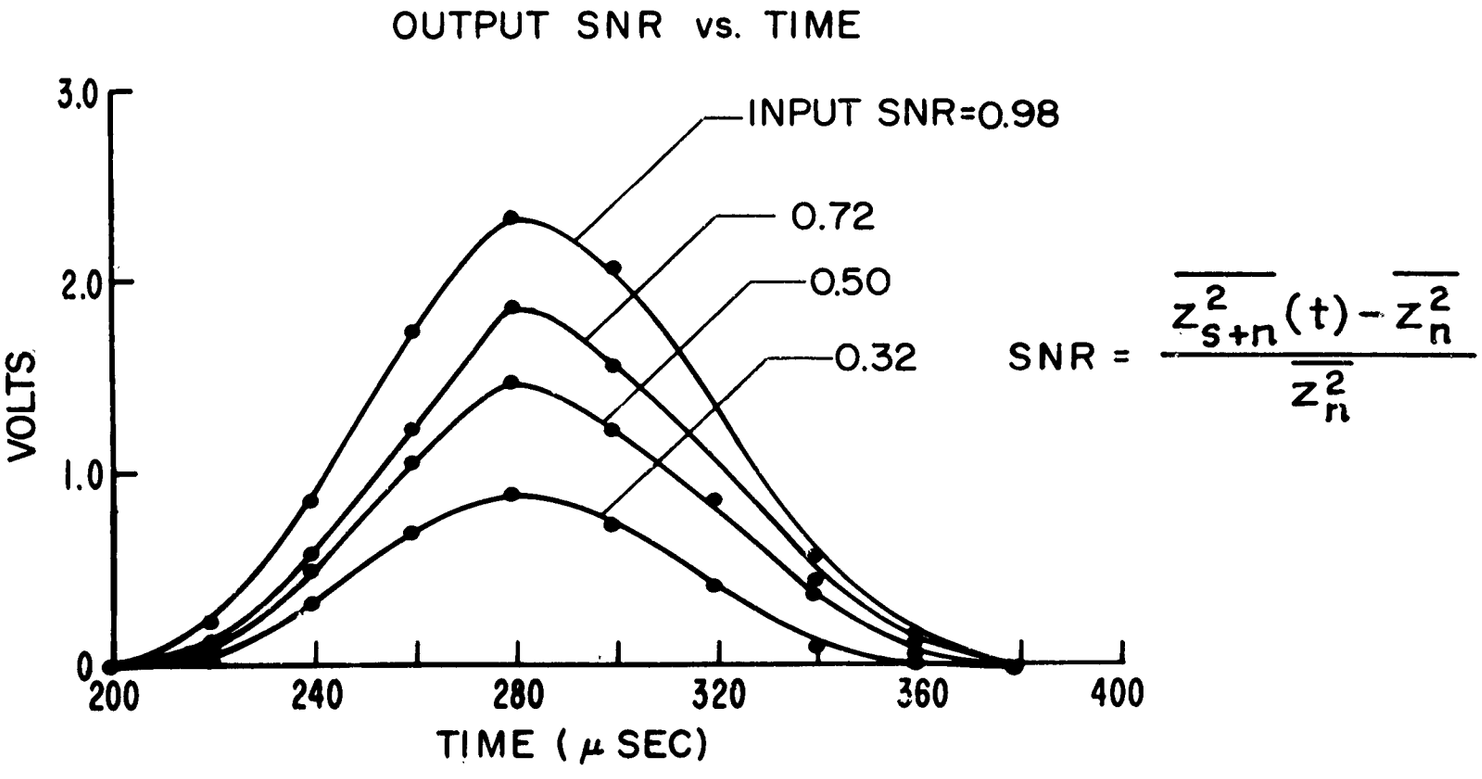

FIG. 27 OUTPUT SNR FOR HALF-WAVE LINEAR DEVICE.

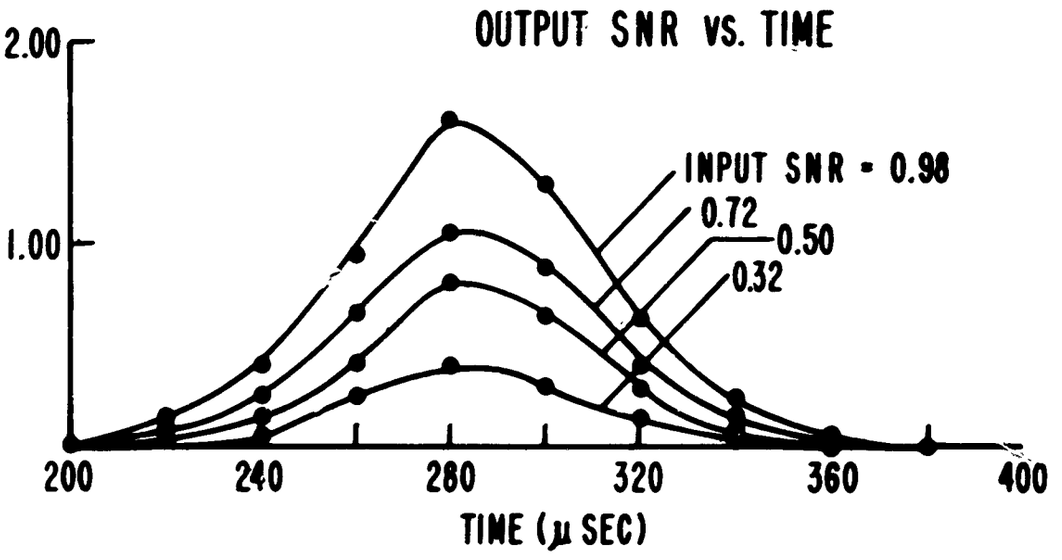

FIG. 28 OUTPUT SNR FOR HALF-WAVE LINEAR DEVICE WITH CLIPPING.

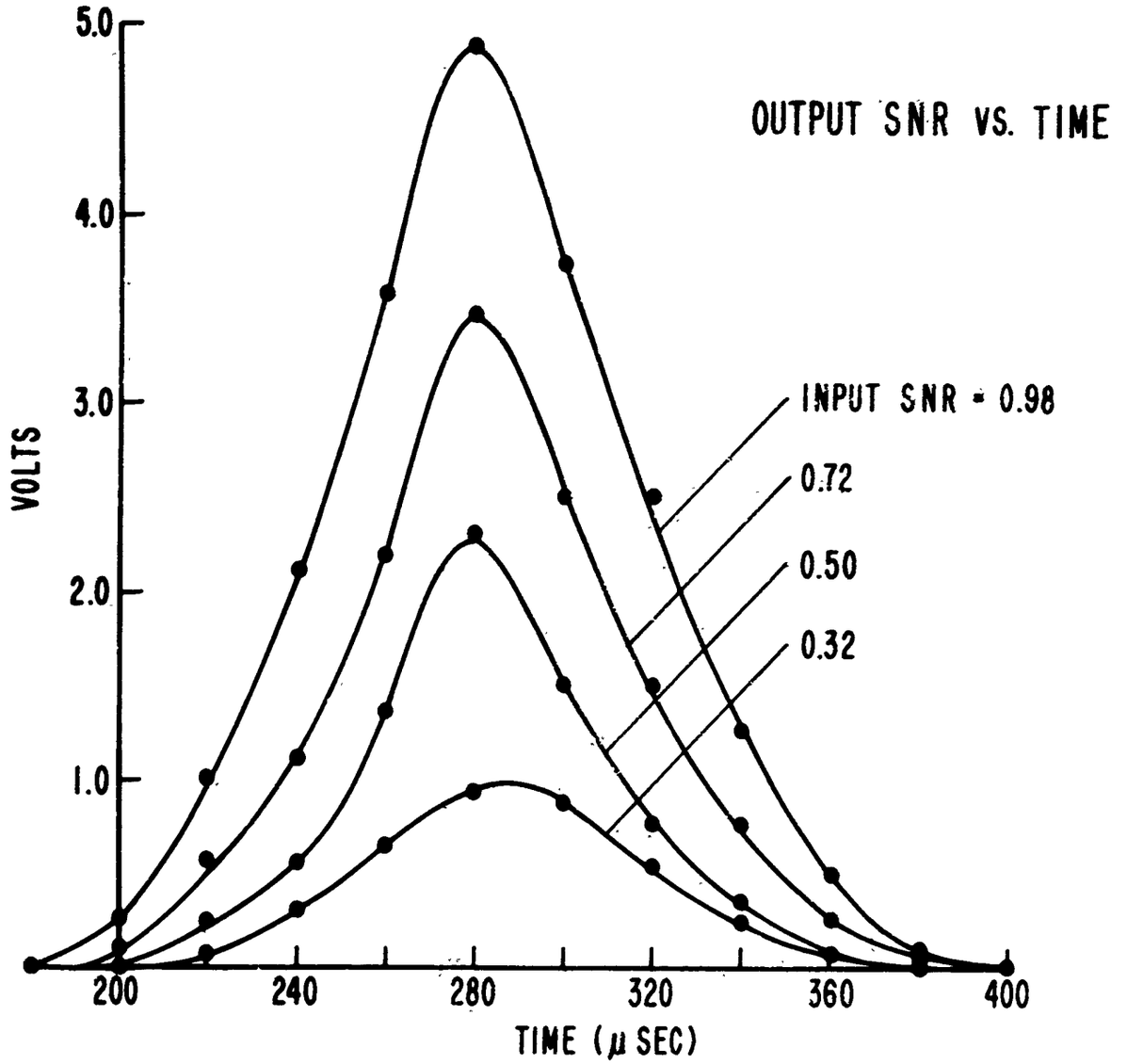

FIG. 29 OUTPUT SNR FOR HALF-WAVE SQUARE LAW DEVICE.

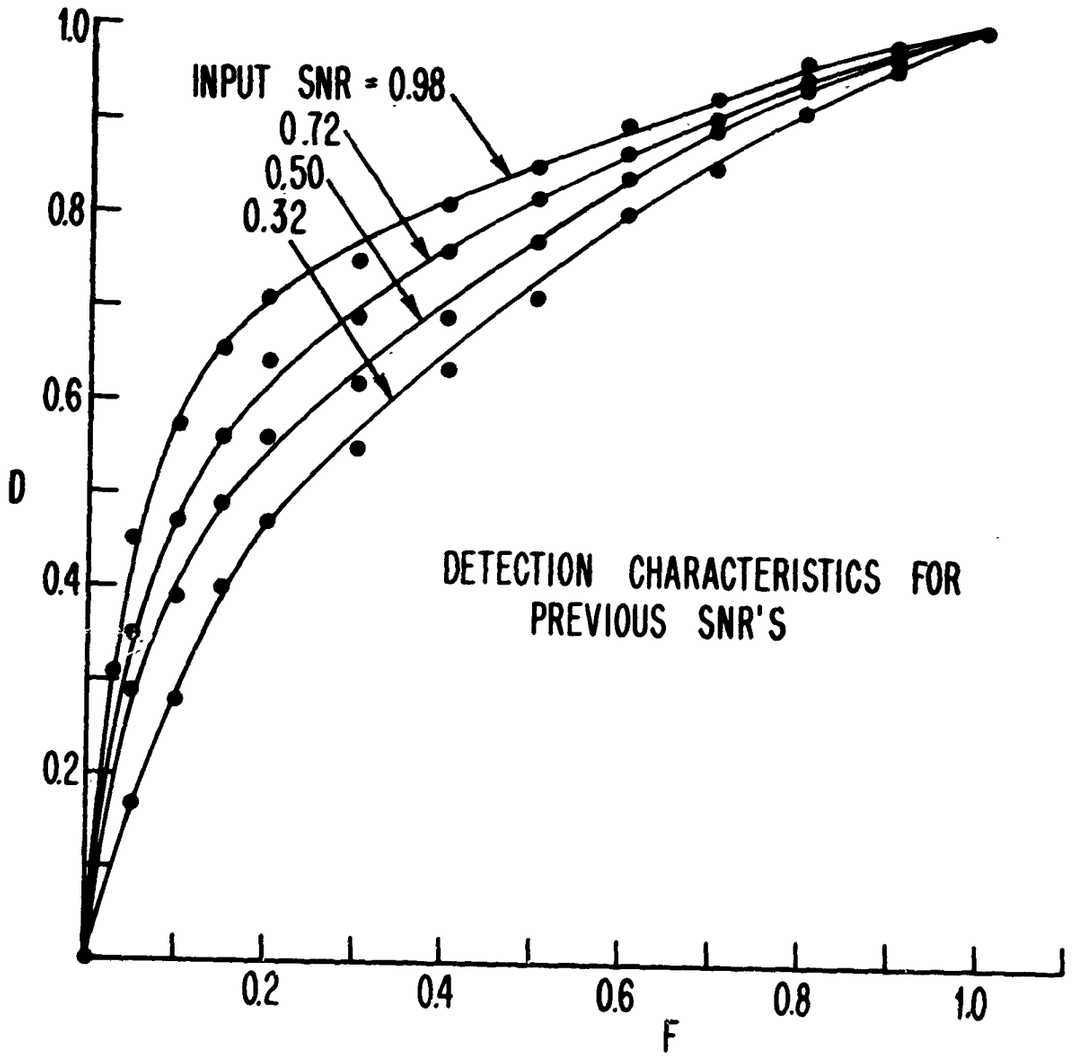

FIG. 30 DETECTION CHARACTERISTICS FOR HALF-WAVE LINEAR AND SQUARE LAW DEVICES.

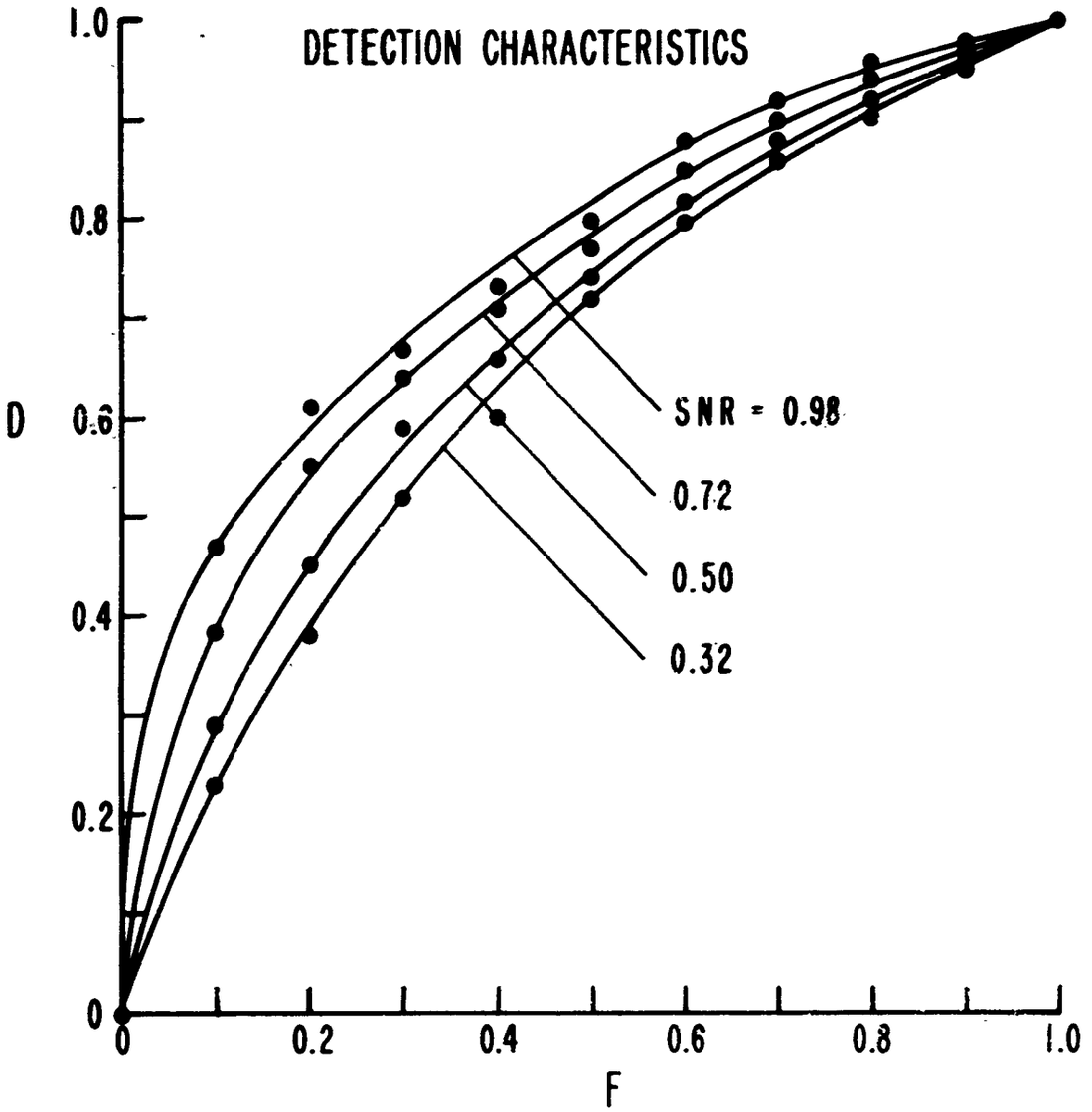

FIG. 31 DETECTION CHARACTERISTICS FOR HALF-WAVE LINEAR DEVICE WITH CLIPPING.

REFERENCES

1. S. O. Rice, Mathematical Analysis of Random Noise, " Selected Papers on Noise and Stochastic Processes, Edited by Nelson Wax, Dover 1954.

2. W. B. Davenport, Jr. and W. L. Root, Introduction to Random Signals and Noise, New York: Mc Graw-Hill Book Co., 1958.

3. M. Kac and A. J. F. Seigert, J. Appl. Phys, 18, 383-397 (1947).

4. A. J. F. Seigert, Trans IRE PGI 7, vol. 3 (1954).

5. R. C. Emerson, J. Appl. Phys. 24 (1953).

6. C. N. Berglund, "A Note on Power Low Devices and Their Effect on Signal-to-Noise Ratio, Trans. IEEE PGI 7, vol. IT-10 (January 1964).

7. N. M. Blochman, "Band-Pass Nonlinearities," Trans IEEE PGI-7, vol. IT-10 (April 1964).

8. D. Middleton, Introduction to Statistical Communication Theory, New York: Mc Graw-Hill Book Co., 1960.

9. L. A. Wainstein and V. P. Zubakov, Extraction of Signals from Noise, Englewood Cliffs, New Jersey: Prentice Hall, Inc., 1962.

BASIC TR DISTRIBUTION LIST

Director of Defense Research & Engineering
The Pentagon
Washington, D. C. 20301*

Chief of Naval Operations
Department of the Navy
Washington, D. C. 20350
Attn: OP-96

Chief of Naval Operations
Department of the Navy
Washington, D. C. 20350
Attn: OP-32

Chief of Naval Operations
Department of the Navy
Washington, D. C. 20350
Attn: OP-07T

Chief of Naval Operations [2]
Department of the Navy
Washington, D. C. 20360
Attn: Code 427, Dr. A. Shostak

Chief of Naval Research
Department of the Navy
Washington, D. C. 20360
Attn: Code 421

The Director [6]
Naval Research Laboratory
Washington, D. C. 20390
Attn: Technical Information Office
Code 2627

Martin A. Garstens
Physics Branch, Code 421
Office of Naval Research
Washington, D. C. 20360

Bureau of Ships, Code 673
Department of the Navy
Washington, D. C. 20360

Defense Documentation Center
Cameron Station [20]
Alexandria, Virginia 22314
Attn: DDC-IRA

Commanding Officer [10]
Office of Naval Research Branch Office
Navy 100, Box 39
Fleet Post Office
New York, New York 09599

Commanding Officer [2]
Office of Naval Research
495 Summer Street
Boston, Massachusetts 02110

Commanding Officer
Office of Naval Research
230 N. Michigan Avenue
Chicago, Illinois 60601

Commanding Officer
Office of Naval Research
207 West 24th Street
Pasadena, California 91101

Commanding Officer
Office of Naval Research
Branch Office
1000 Geary Street
San Francisco, California 94109

Commanding Officer and Director [2]
U. S. Navy Electronics Laboratory
San Diego, California 92152
Attn: Library

Commanding Officer
U. S. N. Air Development Center
Johnsville, Pennsylvania 18974
Attn: NADC Library

Commander
U. S. Naval Weapons Laboratory
Dahlgren, Virginia 22448

Commander
U. S. Naval Ordnance Laboratory
White Oak, Silver Spring
Maryland 20910

Librarian
U. S. Naval Post Graduate School
Monterey, California 93940
Attn: Technical Reports Section

Director [19]
U. S. Army Electronics Laboratories
Fort Monmouth, New Jersey 07703
Attn: AMSEL-RD-DR AMSEL-RD-PE

(Distribute one copy to each)		
	C	PF
	CD	PR
	CF	S
	ND	SA
	NE	SE
	NP	SR
	NR	SS
	P	ADT
		FUPI

Commanding General
U. S. Army Electronics Command
Fort Monmouth, New Jersey 07703
Attn: AMSEL-SC

Director
U. S. Army Electronics Laboratories
Fort Monmouth, New Jersey 07703
Attn: Mr. Robert O. Parker
(AMSEL-RD-X)
Executive Secretary, JSTAC

Director
U. S. Army Electronics Laboratories
Fort Monmouth, New Jersey 07703
Attn: Dr. S. Benedict Levin, Director
Institute for Exploratory Research

Director
U. S. Army Electronics Laboratories
Fort Monmouth, New Jersey 07703

Commanding General
U. S. Army Materiel Command
Washington, D. C. 20315
Attn: AMCRD-RS-PE-E

Commanding General
U. S. Army Strategic Communications Command
Washington, D. C. 20315

Commanding General
Limited Warfare Laboratory
Aberdeen Proving Ground
Aberdeen, Maryland 21005
Attn: Technical Director

Commanding Officer
U. S. Army Ballistics Research Laboratory
Aberdeen Proving Ground
Aberdeen, Maryland 21005
Attn: V. W. Richards

Commanding Officer
Human Engineering Laboratories
Aberdeen Proving Ground
Aberdeen, Maryland 21005

Commanding Officer
U. S. Army Materials Research Agency
Attn: AMXMR-ATL
Watertown, Massachusetts 02172

Commanding Officer
U. S. Army Engineers
Research and Development Laboratories
Fort Belvoir, Virginia 22060
Attn: Technical Documents Center

Director
U. S. Army Engineer Geodesy
Intelligence and Mapping
Research and Development Agency
Fort Belvoir, Virginia 22060

Commanding Officer
U. S. Army Engineers
Research and Development Laboratory
Fort Belvoir, Virginia 22060
Attn: STINFO Branch

Commanding Officer
Harry Diamond Laboratories
Connecticut Ave. and Van Ness St., N. W.
Washington, D. C. 20438
Attn: Mr. Berthold Altman

Commanding Officer
Harry Diamond Laboratories
Connecticut Ave. and Van Ness St., N. W.
Washington, D. C. 20438
Attn: Library

Chief of Research and Development
Headquarters, Department of the Army
Washington, D. C. 20310
Attn: Physical Sciences Division P&E

Commandant
U. S. Army Air Defense School
Attn: Missile Science Div., C&S Dept.
P. O. Box 9390
Fort Bliss, Texas 79916

Commanding General
U. S. Army Missile Command
Redstone Arsenal, Alabama 35809

Commanding General
Frankford Arsenal
Philadelphia, Pennsylvania 19137
Attn: SMUFA-1310, Dr. Sidney Ross

Commanding Officer
Picatinny Arsenal
Dover, New Jersey 07801
Attn: Technical Information Branch

U. S. Army Command and
General Staff College
Library Division
Fort Leavenworth, Kansas 66027

Superintendent
U. S. Army Military Academy
West Point, New York 10996

The Walter Reed Institute of Research
Walter Reed Army Medical Center
Washington, D. C. 20012

Mr. A. D. Bedrosian
U. S. Army Electronics Laboratories
Signal Corps Liaison Office
Building 26 - Room 131
Massachusetts Institute of Technology
Cambridge, Massachusetts 02139

Commanding Officer
U. S. Army Electronics R&D Activity
Fort Huachuca, Arizona 85613

Commanding Officer
U. S. Army Signal Missile Support Agency
White Sands Missile Range
White Sands, New Mexico 88002
Attn: SIGWS-MEW
Mr. T. S. Bellows

Commanding Officer
U. S. Army Electronics R&D Activity
White Sands Missile Range
New Mexico 88002

U. S. Army Research Office - Durham
P. O. Box CM, Duke Station
Durham, North Carolina 27706
Attn: Dr. H. Robl, Deputy Director

Commanding Officer
U. S. Army Research Office - Durham
Box CM, Duke Station
Durham, North Carolina 27706
Attn: CRD-AA-IP, Mr. Ulsh

Dr. Chalmers W. Sherwin
Deputy Director (Research & Technology)
OSDR & E
Room 3E-1060, The Pentagon
Washington, D. C. 20301

Dr. Edward M. Reilley
Assistant Director (Res)
Office of Defense Res & Eng
Department of Defense
Washington, D. C. 20301

Dr. James A. Ward
Office of Deputy Director
Research and Information, Rm. 3D 1037
Department of Defense
The Pentagon
Washington, D. C. 20301

Chief of Research and Development
Headquarters, Department of the Army
Washington, D. C. 20301
Attn: Physical Sciences Division P & E

Research Plans Office
U. S. Army Research Office
3045 Columbia Pike
Arlington, Virginia 22204

Department of the Army
Foreign Service and Technology Center
Munitions Building
Washington, D. C. 20315

Commanding Officer
U. S. Army Security Agency
Arlington, Virginia 22212

Director
Advanced Research Projects Agency
Department of Defense
Washington, D. C. 20301

Mr. Charles Yost
Advanced Research Projects Agency
Department of Defense
Washington, D. C. 20301

Headquarters
Air Research and Development Command
Andrews Air Force Base
Washington, D. C. 20331

Air Force Office of Scientific Research
Washington, D. C. 20333
Attn: SRPP

Air Force Systems Command (SC TR)
Andrews Air Force Base
Washington, D. C. 20331

Hq. AFCRL (CRXL)
L. G. Hanscom Field
Bedford, Massachusetts 01731
[2] CRXL
[1] CRR-Dr. Nollingsworth
[1] CRF
[1] CRW

6570 AMRL (MRRSL, Library)
Wright-Patterson Air Force Base
Ohio 45433

Director, Air University [2]
Library
Maxwell Air Force Base, Alabama 36112

AFMTC Technical Library
Patrick Air Force Base, Florida 32925

RADC (EMILAL-1)
Griffiss Air Force Base, New York 13442
Attn: Documents Library

Director
National Security Agency
Fort George Meade, Maryland 20755
Attn: R4, Dr. H. Campaigne

National Security Agency
Physical Sciences Division
Fort George Meade, Maryland 20755
Attn: Dr. Alvin Meckler

AFWL (WLIL)
Kirtland Air Force Base
New Mexico 87117

Systems Engineering Group
Deputy for Systems Engineering
Directorate of Technical Publications and
Specifications (SEPAR)
Wright-Patterson Air Force Base
Ohio 45433

Air Force Institute of Technology Library
AFIT-LIB Building 125, Area B
Wright-Patterson Air Force Base
Ohio 45433

Microwave Laboratory
Stanford University
Stanford, California 94305
Attn: Librarian

Sandia Corporation
ORG. 1425 Sandia Base
Albuquerque, New Mexico 87115
Attn: Technical Library

Sandia Corporation
P.O. Box 5800
Sandia Base
Albuquerque, New Mexico 87115
Attn: Technical Library

Librarian
U. S. Department of Commerce
National Bureau of Standards
Boulder, Colorado 80301

Librarian
National Bureau of Standards
Room 301, Northwest Building
Washington, D. C. 20234

U. S. Coast Guard
1300 E Street N. W.
Washington, D. C. 20226

Battelle Memorial Institute
505 King Avenue
Columbus, Ohio 43201
Attn: C. J. Falbenbach

Stanford Electronics Laboratory
Stanford University
Stanford, California 94305
Attn: Document Library
Applied Electronics Laboratory

Engineering Division
Case Institute of Technology
Cleveland, Ohio 44106
Attn: H. R. Nara
Associate Director

Antenna Laboratory
Department of Electrical Engineering
The Ohio State University
2024 Neil Avenue
Columbus, Ohio 43210
Attn: Reports Librarian

Polytechnic Institute of Brooklyn
Graduate Center Library
Route 110
Farmingdale, L. I., New York 11735

The University of New Mexico
Department of Electrical Engineering
Albuquerque, New Mexico 87106

Carlyle Barton Laboratories
Johns Hopkins University
Charles and 34th Street
Baltimore, Maryland 21218

Prof. A. W. Lawson
Department of Physics
University of California
Riverside, California 92502

Massachusetts Institute of Technology
Engineering Library
Building 10 - Room 250
Cambridge, Massachusetts 02139
Attn: Technical Reports Collection

Massachusetts Institute of Technology
Research Laboratory of Electronics
Document Office, Building 26, Room 327
Cambridge, Massachusetts 02139
Attn: Mr. John Hewitt

Massachusetts Institute of Technology
Lincoln Laboratory
P. O. Box 73
Lexington, Massachusetts 02173
Attn: Library A-082

Advisory Group on Electron Devices
346 Broadway, 8th Floor
New York, New York 10013

Charles C. M. Tung
Bell Telephone Laboratories 2D-347
Murray Hill, New Jersey 07971

Research Materials Information Center
Oak Ridge National Laboratory
P. O. Box X
Oak Ridge, Tennessee 37831

Institute of Science and Technology
The University of Michigan
P.O. Box 618
Ann Arbor, Michigan 48107
Attn: William Wolfe
Group Supervisor, IRIA

Via: ONR Representative (Mr. R.P. Thacher)
Research Administration Building
The University of Michigan
Ann Arbor, Michigan 48105

Chung Kung University
Department of Electrical Engineering
Tainan, Taiwan
Republic of China
Attn: Prof. Chao-Hsi-Chou
Head, English Department

Gordon McKay Library [2]
Pierce Hall, Harvard University
Cambridge, Massachusetts 02138
Attn: Technical Reports Collection

Editorial Office [4]
Pierce Hall 210, Harvard University
Cambridge, Massachusetts 02138
Attn: Technical Reports Reserve

Assoc. Dean F. K. Willenbrock
Pierce Hall 214, Harvard University
Cambridge, Massachusetts 02138

Prof. R. W. P. King [4]
301 Gordon McKay Laboratory
Harvard University
Cambridge, Massachusetts 02138

Dr. Daniel Alpert, Director
Coordinated Science Laboratory
University of Illinois
Urbana, Illinois 61803

Prof. Z. A. Kaprielian
Electronics Sciences Laboratory
University of Southern California
Los Angeles, California 90007

Dr. Robert Novick, Director
Columbia Radiation Laboratory
Columbia University
538 West 120th Street
New York, New York 10027

Prof. D. J. Angelakos
Acting Director
Electronics Research Laboratory
University of California
Berkeley, California 94720

Prof. A. A. Dougal
Department of Electrical Engineering
University of Te. .s
Austin, Texas 78712

Contract Nonr-1866(38) ONLY

Department of Electrical Engineering
King's College
Newcastle upon Tyne
England

National Aeronautics and Space Administration
Langley Research Center
Langley Station
Hampton, Virginia 23365
Attn: Mrs. Elisabeth R. Gilman, Librarian
Mail Stop 185

Contract Nonr-1866(38) ONLY

U. S. Atomic Energy Commission
Division of Technical Information Extension
P. O. Box 62
Oak Ridge, Tennessee 37831

---

*One copy to each address, unless otherwise indicated by numbers enclosed in brackets.